

Politecnico di Torino

Master's degree in Biomedical Engineering



Development of microfluidic devices using 3D printing for cell culture and drug testing

Supervisor:

Dott. Ignazio Roppolo

Co-Supervisor:

Dott.ssa Francesca Frascella

Candidate:

Chiara Santamaria

s300927

Academic year 2023/2024

ABSTRACT

Cell culturing and in vitro testing are the cornerstone investigations that allowed the development of medicine and biology in the last century. Nevertheless, the most of studies requires a series of operations that involve manual handling of liquid substances through pipetting devices. Those, in addition to being highly time-consuming, are accompanied by the possibility of errors related to the manual dexterity and experience of the operator. Therefore, it clearly emerged the necessity to develop smart biomedical devices that may help end-users to save time and enable more controlled procedure. Automatic pipetting helped to face this problem, but on the other hand the complexity of in-vitro studies still request considerable human efforts. In this context, multiwell plates, also known as microwell plates or multiwells, are the basic tools for performing such experiments. Smart multiwell systems, in which different wells are connected by microfluidic channels, would allow for the reduction of manual operations. In this way, the manual pipetting of samples into the wells is completely replaced by the presence of a microfluidic system that connects the various wells and is, in turn, connected to a pumping system. This allows for the automation of cell proliferation and/or drug response tests, optimizing execution times and minimizing operator intervention. Nevertheless, the fabrication of these smart devices is mainly performed by injection molding, i.e. defined geometries are produced, which limit the freedom of automation of experiments.

To make a further step in this direction, the aim of this thesis is to produce a smart plate using additive manufacturing (AM) techniques, which allow the creation of complex geometries from a CAD model which can be user-defined. Specifically, for the development of this device, Digital Light Processing (DLP) was chosen. DLP is a technique that belongs to the vat photopolymerization class, where polymerization of the resin in the vat is induced through irradiation (UV or visible light) and allows high precision and superior complexity when compared to other AM technologies. For the fabrication of the smart plate, two different resins were selected: one that promotes cell adhesion, poly(ethylene glycol) diacrylate 250 (PEGDA 250), and one that inhibits it without inducing cytotoxic effects (TEGORad 2800). Specifically, the base of the object and the bottom of the wells were made with PEGDA, while the channels and wells were made with TEGORad.

Once the device was obtained, microfluidic simulations were conducted using Comsol software, which allowed to simulate various flow rates permitted by the two-head peristaltic pump. Simulation tests were then reproduced in real experiments to verify the reliability of these tests.

Finally, studies were conducted for verifying the cytocompatibility of the material and biological studies on cell viability. For the cell viability study, tests were conducted with three different cell types: human fibroblasts (HFF1), keratinocytes (HaCaT), and endothelial cells (EC).

The successful implementation of this strategy opens to new possibilities of automated, large-scale studies, leaving at the same time the design-of-experiment freedom to investigators.

INDEX

CHAPTER 1: ADVANCED MULTIWELL DEVICES FOR CELL CULTURE AND DRUG TESTING.....	8
1.1 CELL CULTURE: background and challenges.....	8
1.2 IN VITRO DRUG TESTING: background and challenges.....	12
1.3 MICROFLUIDIC AND 3D PRINTING FOR CELL CULTURE AND ADVANCED DRUG TESTING	15
1.4 EXAMPLE OF MULTIWELL PLATES WITH INTEGRATED MICROFLUIDIC: FABRICATION AND APPLICATIONS	18
CHAPTER 2: ADDITIVE MANUFACTURING AND 3D PRINTING	22
2.1 ADDITIVE MANUFACTURING	22
2.2 3D PRINTING	23
2.3 3D PRINTING TECHNOLOGIES AND MATERIALS.....	24
2.3.1 3D-PRINTING TECHNOLOGIES	24
2.3.2 3D- PRINTING MATERIALS.....	28
2.4 PHOTOPOLYMERIZATION FUNDAMENTALS AND LIGHT-INDUCED 3D PRINTABLE FORMULATIONS	30
2.4.1 3D VAT PHOTOPOLYMERIZATION: SLA AND DLP	32
2.5 BIOMEDICAL CONSTRAINTS OF VAT 3D PRINTED DEVICES	34
CHAPTER 3: MATERIALS AND METHODS.....	36
3.1 MATERIALS.....	36
3.2 DLP 3D PRINTER.....	39
3.3 PREPARATION OF FORMULATIONS.....	40
3.3.1 PEGDA	40
3.3.2 TEGORAD	40
3.4 WASHING PROTOCOL AND STERILIZATION PROTOCOL	40
3.5 CHARACTERIZATION METHODS.....	41
3.5.1 FLUIDICS ASSESMENT OF THE SYSTEM PERFUSION	41
3.5.2 UV/VISIBLE SPECTROSCOPY	43
3.5.3 CYTOTOXICITY	45
3.5.4 ASSESMENT OF FEASIBILITY OF THE PLATE TO ANALYZE CELLULAR ASSAYS	46
3.5.5 CELL VIABILITY AND PROLIFERATION	47
3.5.6 FIRST TRIALS OF PERFUSED 3D GeIMA HYDROGEL SCAFFOLDS	48

CHAPTER 4: RESULTS	50
4.1 SOLIDWORKS DESIGN	50
4.2 FORMULATIONS	50
4.2.1 PEGDA FORMULATION	54
4.2.2 TEGORad FORMULATION	55
4.3 PRINTING PARAMETERS OPTIMIZATION	55
4.4 WASHING PROTOCOL	64
4.5 MICROFLUIDIC SIMULATIONS AND TESTS	69
4.6 BIOLOGICAL CHARACTERIZATIONS AND TESTS	80
4.6.1 FLUORESCENCE	80
4.6.2 CYTOTOXICITY	81
4.6.3 INTERACTION BETWEEN MATERIAL AND CELLULAR ASSAY	88
4.6.4 VITALITY AND CELL PROLIFERATION	90
4.6.5 GeIMA HYDROGEL SCAFFOLDS	93
CHAPTER 5: CONCLUSIONS	96
REFERENCES	98

CHAPTER 1: ADVANCED MULTIWELL DEVICES FOR CELL CULTURE AND DRUG TESTING

1.1 CELL CULTURE: background and challenges

Cell cultures are systems in which cells are isolated from their natural environment, and continue their life process within a well-defined parameters. This cell-life condition, known as "in vitro", represent a fundamental tool for the study and for understanding of cell biology, tissue morphology, the mechanisms of various diseases and the action of drugs.

The history of cell cultures traces its roots back to 1907, when Harrison performed the first cell cultures during his research on the origin of nerve fibers. Since then, the advancement of biotechnologies, materials (both natural and artificial), and various culture media has led to the improvement and refinement of the method, making it possible to observe cell growth and differentiation outside the body. [1]

Nowadays, it is possible to classify cell cultures into two main families: two-dimensional culture systems and three-dimensional culture systems.

2D culture systems are characterized by a relatively simple structure composed of a single layer of cells (monolayer) placed in a specific nutrient-rich basal medium that allows for their proliferation. Specifically, the cells under investigation are placed inside a glass or plastic sterile container, e.g. Petri dish, that provides mechanical support. A fundamental aspect of cell cultures is the maintenance of culture conditions: it is necessary to ensure thermal stability, pH level and complete sterility of the medium. This latter aspect is crucial to avoid the presence of microorganisms that could secrete toxic substances harmful to the cells.

Growth in two-dimensional monolayers ensures that cells receive nearly identical amounts of nutrients, which guarantees homogeneous development. This characteristic, combined with simplicity and high efficiency, makes the use of such models very appealing in biomedical research.

2D in vitro models can be used for various applications. It is possible to study certain cellular processes that, under specific controlled conditions, can provide information about the behaviour of the cell line. They can also be employed in the study of the

molecular mechanisms of a pathology, with the aim of identifying the characteristics underlying the onset of the disease and the subsequent progression of a specific illness. [2]

Finally, they can be used in the field of "drug discovery," which involves testing the effects of various chemical and pharmaceutical compounds on specific cell types.

Despite their various applications, 2D cell cultures remain a relatively limited tool because it is very difficult to mimic the immense complexity of the human body with such simple models. In vivo, the cellular microenvironment is rich in factors that influence cellular behavior, such as pH, the presence of ions, soluble factors, and more. Due to their simplicity and the lack of a complex, information-rich environment, 2D systems cannot replicate the cellular development processes observable in physiological contexts. [3] Therefore, they serve as a good starting point for obtaining information that remains general and must be supplemented by further observations made in more specific models, such as 3D models or directly in vivo. [4] Nevertheless, although these limitations are real and challenging to overcome, 2D models continue to be used in various research areas due to their cost-effectiveness and ease of reproducibility. [5]

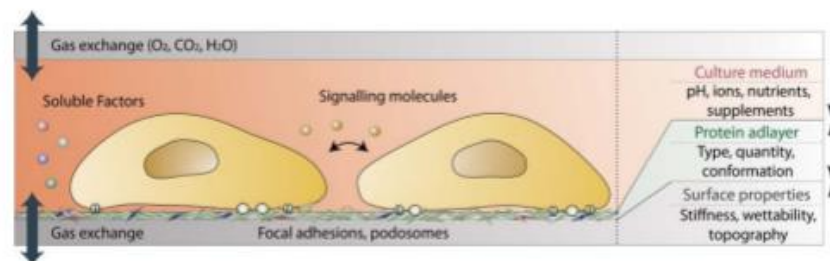


Figure 1. Cellular microenvironment in vitro.

It is precisely because of these limitations that the introduction of more complex tools, such as 3D models, is becoming of paramount importance. This transition has been of crucial in the field of biomedical research because these models allow for cell culture growth that more closely resembles what occurs in vivo. [6]

Cells within our bodies aggregate to create tissues, which in turn form organs. Therefore, the ability to represent such structures is essential for conducting more specific studies of what happens in a particular tissue and/or organ when a certain physiological or pathological condition develops or spreads. Reproducing the

human body remains a challenge for physicians, biologists, and bioengineers who have been striving for years to represent the mechanisms occurring in both healthy and diseased tissues. [7]3D cell culture aims exactly at this goal.

An important aspect for the development of systems capable of achieving tissue-like cellular organization is the presence of various factors influencing cellular behavior, such as the architecture of the extracellular matrix (ECM), its composition, mechanical properties, and numerous interactions among these elements. In standard two-dimensional models, cells are cultured on a surface with higher rigidity (e.g., plastic Petri dish, approximately 105 kPa) compared to the ECM rigidity of tissues, which ranges from 1 to 25 kPa. Different rigidity induces different cytoskeletal conformations, affecting cellular polarity, metabolism, and protein expression. The turning point in 3D culturing was therefore determined by the ability to produce systems that mimic tissue-specific ECM, inducing cellular differentiation and organization resembling that of the tissue under study. [5]

From the initial discovery of the possibility to reproduce a specific environment mimicking the in vivo model, the 3D approach has immediately begun to capture the attention of the researchers. A 3D culture can be defined as "a culture that can mimic the organization and microarchitecture of a living organ," making it indeed a much closer tool to the in vivo model compared to the previously mentioned 2D models. [8]

In these systems, cells can grow within a three-dimensional structure using various supports, which can be synthetic, such as ceramics, metals and polymers, or natural, such as polysaccharides, proteins, ECM derivatives or hydrogels. Alternatively, cells can also grow freely in systems called spheroids and organoids. [6]

The 3D models, besides being innovative in the field of biomedical research, also represent an innovative method in the pharmaceutical and cosmetic industries. Among the potential applications, "drug discovery" is certainly one of the most relevant. In this context, three-dimensional cultures offer the possibility of obtaining more specific and reliable results compared to the exclusive use of two-dimensional systems. The additional dimension of 3D cultures not only influences the spatial organization of surface cellular receptors but also imposes physical constraints on the cells themselves. These spatial and physical aspects in 3D cultures affect signal

transduction from the outside to the inside of the cells and, consequently, gene expression and related cellular behaviours. This leads to obtaining pharmacological treatment responses more like what occurs in vivo. [9]

The following table shows the differences between a 2D culture system and a 3D culture system, highlighting the advantages and disadvantages of using both types of systems:

Features	2D Culture System	3D Culture System
<i>Cell shape</i>	Flat and elongated Mono-layer	Normal cell shape Aggregates/Spheroids Multiple layers
<i>Exposure to the medium</i>	All cells receive the same amount of nutrients and growth factors	Not all cells receive the same amount of nutrients and growth factors Possible necrotic core
<i>Cell junction</i>	Less common and accurate than real cell junctions	Common and allow communication between cells
Cell differentiation	None	Well differentiated
Drug sensitivity	Drugs are poorly metabolized Low resistance to drug treatment	Better drug metabolism Greater resistance to drug treatment Better representation of drug effects
Cell proliferation	Cell proliferate at an unnatural rate	Realistic proliferation rate
Expression levels	Gene and protein expressions different from those in in vivo models	Gene and protein expressions similar to those in in vivo models
<i>Costs</i>	Cheaper	More expensive
Cell apoptosis	Greater apoptotic effects	Lesser apoptotic effects

Table 1. Differences between 2D Culture System and 3D Culture System

1.2 IN VITRO DRUG TESTING: background and challenges

Over the past 30 years, the process of drug discovery and development has become increasingly expensive and risky.

Generally, for the commercialization of drugs (or medical devices), it is necessary to follow specific sequential processes to validate them.

The drug must pass through two phases to be marketed: the preclinical phase and the clinical phase. In the preclinical phase, simplifications are made compared to the human body. In this phase, studies on the drug to be commercialized are conducted outside the physiological environment: animal models and in vitro models are used. In the clinical phase, we can distinguish four sub-phases:

1. Phase 1 involves studying the safety of the drug in a limited population of healthy individuals.
2. In Phase 2, the efficacy of the drug is evaluated in a larger population.
3. Phase 3 entails a more thorough study of the drug's efficacy and safety, maximizing the number of participants.
4. Phase 4 involves long-term observation of the product to identify any late side effects (clinical follow-up). [10]

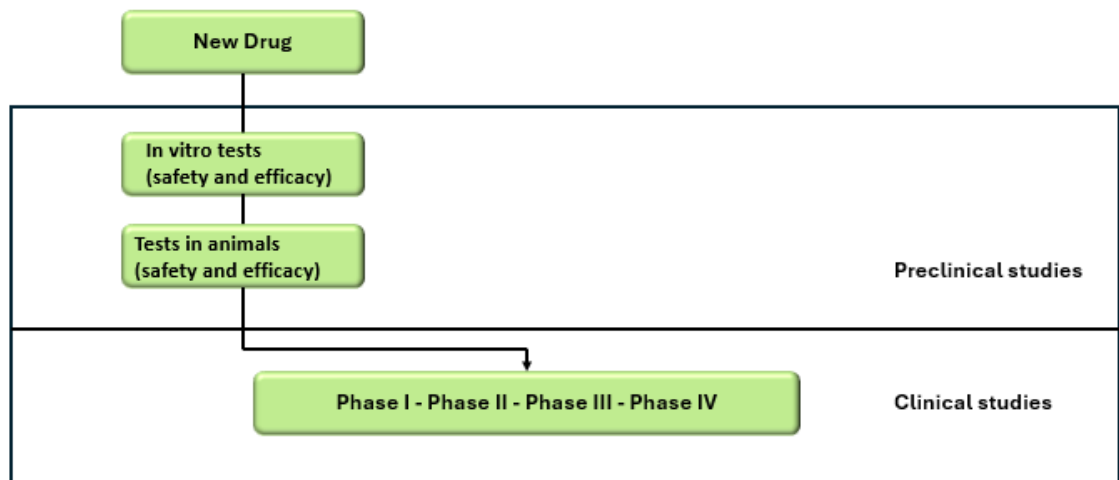


Figure 2. Diagram of drug development

Initially, the main and most widely used method for studying the onset of diseases and testing new drug therapies relied on animal models: indeed, they have a better organization compared to that which can be found in a two-dimensional in vitro

construct. However, there are three main issues associated with the use of animal models:

1. The most significant issue is the *ethical concern*. The use of animals for experimentation in pharmacology and toxicology dates back to the last century and often involves the sacrifice of the animals at the end of the study. The main idea to address this issue is to follow the principle of the 3R. This principle was formulated by British scientists William Russel and Rex Burch in 1959 with the idea of replacing the use of animals in experiments. Since this goal was not immediately achievable, the two scientists encouraged the use of all possible means to improve animal welfare through reduction and refinement. When we talk about the 3R principle, in fact, we are referring to:
 1. **Replacement**: replacing animal material with human material.
 2. **Reduction**.
 3. **Refinement**.

This principle has been included in Directive 2010/63/EU on the protection of animals used for scientific purposes as a legal obligation to be applied to all aspects of the care and use of animals. Guidelines have been provided for EU funding requests for research projects involving animal experimentation. Detailed information must be provided on why live animals need to be used and why that particular choice was made.[11]

2. *Efficacy issue*: Using animal models involves simplifications. The use of animal models involves studying models that have differences both physiologically and anatomically compared to an individual. This is a problem of significant relevance, as especially in the validation of new drugs, many characteristics are lost in the transition from the animal model to the human model, which affects the efficacy of the finding under examination, thus leading to a failure in transitioning to the subsequent phases of the clinical trial, hence not achieving validation.

3. Problem concerning *disease development*. While it is true that some animals can develop certain diseases associated with humans (diseases for which treatments are sought), it is also true that there are other diseases that some animals are unable to develop (such as neurodegenerative and tumor diseases). For this reason, animals requiring genetic modifications to enable them to develop specific diseases should be implemented. However, this often results in outcomes that are not like what would occur in humans. [10]

For the reasons mentioned above, efforts have been made to explore alternatives to the use of animal models (where possible) by developing experimental 2D and 3D models that exhibit biomimetic characteristics, aiming to achieve models that are increasingly similar to the in vivo environment.

In the biomedical field, the most commonly used tools are cell cultures. They can be of human or animal origin and, by seeking to faithfully reproduce tissue at a physiological level, they offer the possibility of studying and investigating various aspects of cellular functions.

Cellular assays thus become the key tool used to assess the potential efficacy of a new compound in drug discovery. To obtain more reliable results, the culture model used as a testing platform must function similarly to cells in vivo.

In the case of 2D cultures, they are only able to represent a "small portion" of the human body, mimicking the disease and how it is intended to be treated to a minimal extent. Therefore, the results of experiments with this type of tool have limitations:

- a. While cells grow well in the laboratory, they are not representative of the variety of cells that make up a tissue.
- b. Cells in culture do not receive signals from other cells in the body that influence their behavior.

Due to these limitations, three-dimensional cellular culture systems are gaining increasing interest in the field of drug discovery. They allow for more specific and reliable results compared to 2D systems. [9] Several studies have shown greater similarity in responses to drug treatments in three-dimensional systems than in two-dimensional ones. They allow for more specific and reliable results than 2D systems.

Indeed, several studies have shown greater similarity in responses to drug treatments in 3D systems. [12] [13]

Although 3D cell cultures have gained increasing attention in drug screening, many currently available 3D culture techniques require a lot of time, are costly, and lack reproducibility. Scientists are thus engaged in developing new rapid standard protocols for the use of three-dimensional cultures in pharmacological screening. [14]

1.3 MICROFLUIDIC AND 3D PRINTING FOR CELL CULTURE AND ADVANCED DRUG TESTING

Microfluidics is defined as the manipulation of fluids in channels with micrometric dimensions; specifically, the width or height of the channels can range from 1 to 1000 μm . These systems allow for the handling of small volumes of fluids, typically in the order of micro or nanoliters. [15], [16]

In the last decade, the use of microfluidics has become increasingly important in biochemical and clinical applications. In particular, one of the areas where it seems to be attracting more attention is drug screening, and this is because nowadays drug discovery is a multibillion-dollar endeavor that requires a significant initial investment in terms of both time and capital, without guaranteeing any success.

Current studies indeed show that the development and study of a drug take approximately 15 years. Despite the high time and costs involved, data indicate that 7 out of 10 drugs do not recoup the research and development (R&D) costs incurred.

This translates into a growing interest in the development of new devices that allow for biochemical experimentation/analysis of drugs on individual living cells using small amounts of fluid. These devices are called microfluidic devices. Using such devices brings the advantages of reducing cell consumption, enabling the automated addition of reagents, and reproducibly mixing reagents with cells. [17]

The Reynolds number (Re) is one of the most important parameters describing the flow in these systems. It is defined as the ratio of inertial forces to viscous forces:

$$Re = \frac{\rho v L}{\mu}$$

With

ρ ($\frac{kg}{m^3}$) fluid density

v ($\frac{m}{s}$) velocity

L (m) characteristic length

μ (Pa s or $\frac{N \cdot s}{m^2}$ or $\frac{kg}{m \cdot s}$) dynamic viscosity

The Reynolds number provides information about the flow regime. We can speak of laminar flow and turbulent flow: in the former case, the flow lines are parallel, while in the latter case, the flow lines are chaotic, and mixing is rapid, uncontrollable, and difficult to calculate.

In microfluidic devices, the Reynolds number is often less than unity, so laminar flows can be observed throughout the device. [18] For the realization of such devices, microfabrication techniques are employed.

This type of production techniques is suitable for creating structures with defined shapes and positions on a micrometer scale that can be used to position cells and tissues, controlling the shape and function of cells in a controlled manner.

Microfabrication has found extensive applications across various domains in biology and medicine. These include the development of tools for molecular biology and biochemistry, advancements in cell biology instrumentation, the creation of medical devices, and the innovation of biosensor technologies.[19]

Soft lithography is the primary technique for manufacturing microfluidic devices. It replaces conventional photolithography, which is still used for creating devices larger than 100 nm in size, in order to achieve micro- and nanofabrication. [20]

Today, 3D printing represents a promising alternative to soft lithography. It allows for the creation of structures with well-defined geometries at a lower cost. The use of this type of technology, for example, eliminates the need to work in cleanrooms. Recent advancements in 3D printing technologies have enabled the production of highly complex microfluidic devices, which can be obtained in a single step or in multiple steps, assembling various components printed in 3D.

This alternative represents a rapid and economical production technique, making microfluidics more accessible to users. [21]

The use of 3D printers for PDMS microfluidic devices is particularly promising for cell culture applications. The printing process does not alter the properties of PDMS, such

as biocompatibility and oxygen permeability, resulting in reduced overall costs and fabrication time. [22]

The low cost, easy surface modification and high gas permeability are the key properties of PDMS that make it a highly popular material for microfluidic-based systems. Its transparency is necessary and useful for users to observe what happens inside the device. [23]

Besides PDMS, 3D printing can be used with other types of resins, both commercial and non-commercial. However, for use in biomedical applications, the microfluidic devices produced must be made from materials that do not react with or absorb protein reagents and nucleic acids. The resins must also be biocompatible, so that when cells come into contact with them, they do not undergo cell death. Currently, many commercial resins are already cytocompatible. [24]

The increasingly widespread adoption of microfluidics is indeed due to the discovery and development of new materials.

With the continuous development of materials and the resulting increase in interest in microfluidics, attention has also been focused on a new concept, that of the organ-on-a-chip.

The term "organ-on-a-chip" refers to a biotechnology that currently represents one of the most promising and exciting developments in the field of microfluidics.

These devices aim to miniaturize and mimic a specific organ. They enable the simulation of crucial physiological signals, such as vascularization, thereby improving the emulation of in vivo physiological conditions for the study of various biological processes.

The main advantages lie in the ability to recreate a controlled and dynamic environment capable of mimicking the mechanical and physiological signals originating from cell cultures, making it a complex environment similar to what we find in the human body. Additionally, these systems have relatively low costs and rapid fabrication times. [11]

These biochips, therefore, emerge as promising candidates to replace animal models currently used in predicting human responses, given the inherent species differences and ethical debates surrounding them. The development of these microchips is associated with the idea that in the future, they may serve as the starting point for drug toxicity testing, leading to a reduction in the number of failures that occur when transitioning from preclinical to clinical studies in drug development. [6]

1.4 EXAMPLE OF MULTIWELL PLATES WITH INTEGRATED MICROFLUIDIC: FABRICATION AND APPLICATIONS

The continuous development of new microfluidic devices and their small dimensions has led to their use in cell culture, testing new drugs, and studying interactions between cells and specific molecules that can occur at the physiological level.

Lee et al. have developed, using stereolithography, a complete device that does not require additional components.

Specifically, they created a device for the detection of pathogenic bacteria consisting of a helical microchannel. The authors used clusters of magnetic nanoparticles functionalized with antibodies capable of binding to *E. coli*. The device features a trapezoidal cross-sectional shape to prevent the accumulation of particles adjacent to the inner walls of the channels.

By utilizing functionalized particles, the authors were able to separate clusters of individual particles from clusters of particles bound to the bacteria based on particle size, achieving a detection limit of 10 cfu/ml in a buffer solution and 10 cfu/ml in milk. [21]

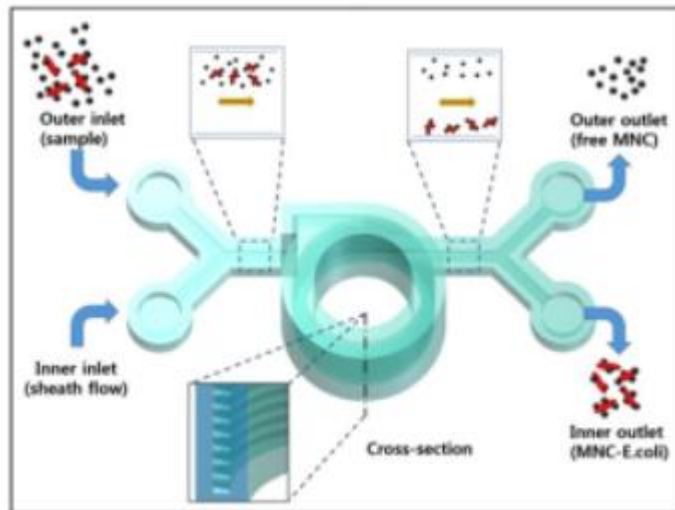


Figure 3. 3D-printed microfluidic system for bacteria detection

In addition to simple cell culture or drug testing, microfluidic devices can also be used to support malfunctioning organs. To address liver dysfunction in patients with liver pathologies, Park et al. developed a bioartificial liver device (BAL) that allows long-term survival of hepatocytes. They designed a radial flow bioreactor to protect the seeded hepatocytes from shear stresses due to metabolic exchange that could be harmful. This device consists of a stack of circular glass substrates with concentric microgrooves in a polycarbonate housing. A peristaltic pump was used to circulate culture medium between the reservoir, oxygenator, and bioreactor. Once the critical shear stress value of 0.33 dyn/cm^2 was identified, it was observed that with a flow rate of 18 ml/min , this threshold was still not exceeded. This device demonstrated that after 36 hours of perfusion, the viability of hepatocytes was around 95% at various radial distances observed (20, 12, and 5 mm) on substrates with microgrooves, while in those without microgrooves, cellular viability ranged from 98% to 0% depending on the observed distances.

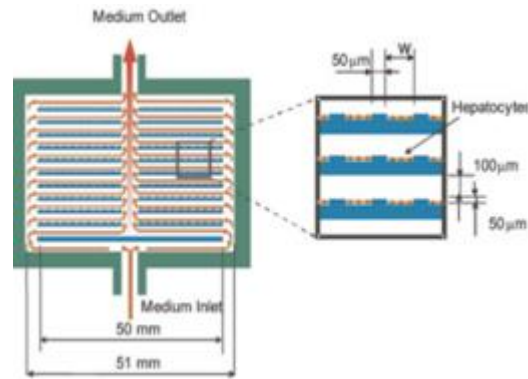


Figure 4. Schematic diagram of the radial-flow bioreactor with microgrooves for 2D culture of Hepatocytes

Based on the architecture of hepatic organs, Carraro et al. developed a two-layer microfluidic device featuring a network of channels mimicking blood vessels in one layer and a parenchymal chamber in the other. The layers were separated by a nanoporous polycarbonate membrane allowing metabolite transfer but protecting hepatocytes from excessive shear stress.

The width of the main inlet and outlet channels is 1650 μm , gradually branching and decreasing to 35 μm .

The fluid was injected into the system using a syringe pump with a flow rate of 0.5 ml/h. With this flow, the device demonstrated the ability to maintain viable hepatic cells, their proliferation, and functionality for 14 days.

Carraro et al. then considered how to further improve the number and vitality of cells by coating the polycarbonate membrane with collagen that mimics the extracellular matrix.

Budoin et al., instead of focusing on the vitality of liver cells, developed a device for studying the cultivation of the HepG3/C3A hepatocarcinoma cell line. The device consists of two layers of PDMS, characterized by microstructures designed to enhance 3D cell culture, on the lower layer. These microstructures consist of microchambers and microchannels placed within a cell culture chamber with a geometry suitable for uniform flow. Inlets and outlets were present in the upper layer.

This device was used to study the metabolic activity of cells at different flow rates of the medium (0.10 and 25 $\mu\text{l}/\text{min}$) to conduct a toxicological analysis. [17]

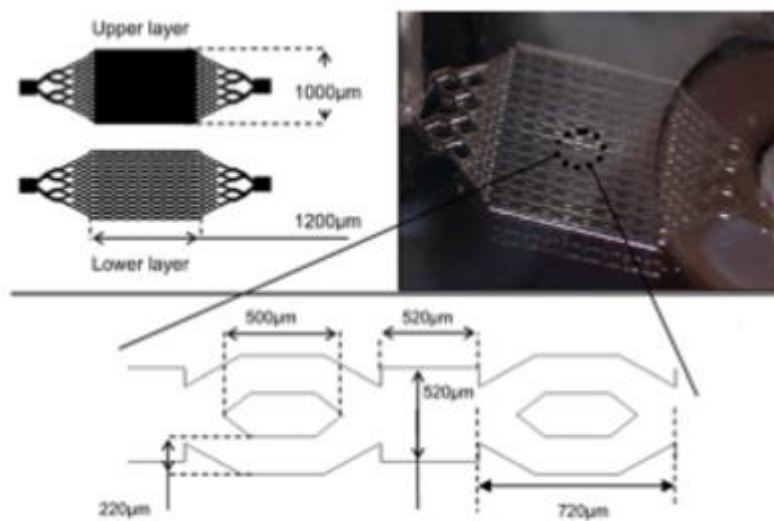


Figure 5. Design of the microfluidic bioreactor for hepatocarcinoma cultivation in 3D cell layers

CHAPTER 2: ADDITIVE MANUFACTURING AND 3D PRINTING

2.1 ADDITIVE MANUFACTURING

The term Additive Manufacturing (AM) refers to a group of technologies that create objects from a three-dimensional model by adding material layer by layer. These types of technologies are distinguished from subtractive manufacturing techniques, where the final product is obtained by removing material. Figure 2.1 shows the differences between the two types of manufacturing. [25]

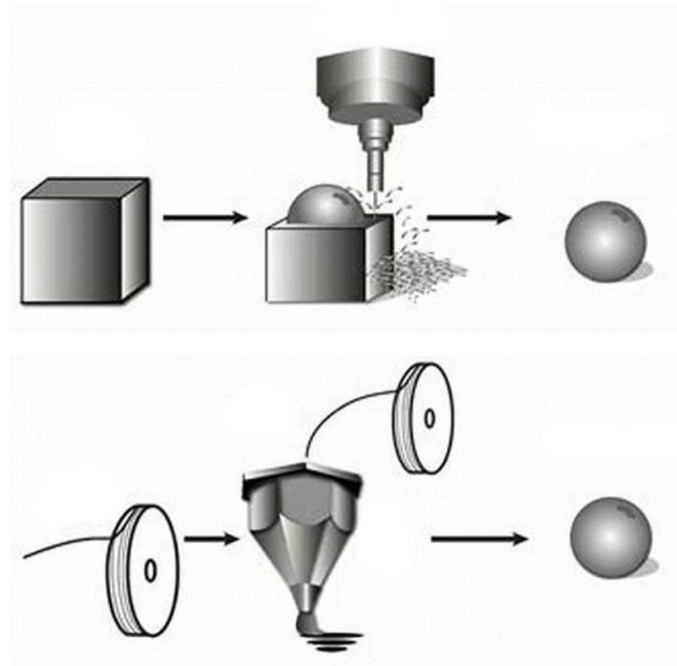


Figure 2.1 Schematic representation of subtractive manufacturing (above) and additive manufacturing (below) [2]

Today, the term Additive Manufacturing is used as synonym of 3D printing, but the latter should be better used to refer to low-cost technologies. The first 3D printing technology was developed by Charles Hull in 1986, who devised a method known as stereolithography. Hull's inventions were followed by subsequent developments of other techniques which employed different build approaches such as powder bed

fusion, inkjet printing, and fused filament fabrication (FFF). Initially, 3D printing was used by engineers and designers who utilized this process for creating aesthetic and functional prototypes due to its capability for rapid and cost-effective fabrication of complex objects. The use of 3D printing has, in fact, minimized the additional costs incurred in the product development process. However, it is only in recent years that 3D printing has gained success across various sectors. The growing acceptance of this manufacturing technique over traditional methods is attributed to numerous advantages, including the fabrication of complex geometries with high precision, material savings, and flexibility in the design and customization of the final object. [26], [27]

2.2 3D PRINTING

To create a physical object through a 3D printing process, several steps need to be followed, as shown in figure number.

First, to produce an object through 3D printing, it is necessary to create a CAD model using specific software. Once the CAD model is created, it is saved in STL format (or other formats supported by the printers). This is followed by the slicing process: the model is divided into layers of appropriate thickness, whose overlapping will lead to the creation of the final object. After this process, the STL file needs to be converted into g-code, which contains all the information for the fabrication of the object. This makes it possible to start the printing process. Once this process is completed, the product must be removed from the printer. At the end of the process, some post-processing steps might be necessary, such as curing, removal of support structures, smoothing of edges, or application of coatings. [28]

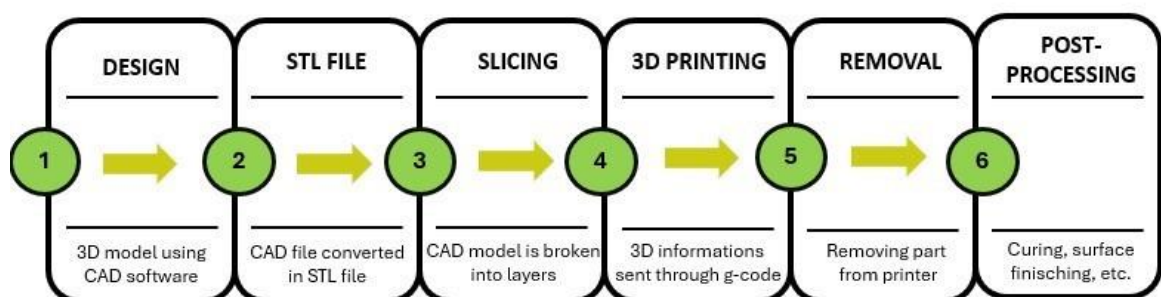


Figure 2.1 Workflow in 3D printing process

Nowadays, there are various 3D printing techniques. The ASTM (American Society for Testing and Materials) has classified the printing processes into seven categories, which are as follows:

1. PBF: Powder Bed Fusion
Thermal energy is used to selectively melt or sinter a bed of powders.
2. ME: Material Extrusion
Material is extruded through a nozzle.
3. MJ: Material Jetting
Similar to 2D inkjet printers, where material is deposited in liquid phase, drop by drop.
4. VP: Vat Photopolymerization
A technique that uses a photopolymerizable resin, which is cross-linked by selectively irradiating it with a laser or another light source.
5. BJ: Binder Jetting
A binder is deposited layer by layer onto a bed of powder material to create the object.
6. SL: Sheet Lamination
Layers of solid material are cut and glued together.
7. DED: Direct Energy Deposition
Thermal energy is used to melt material as it is being deposited.

Each technique can be used depending on the material to be used and the desired final object and its resolution. Depending on the chosen method, different levels of resolution can be achieved, with some techniques providing higher resolution than others. [28], [29] In addition to the variety of printing technologies, the spread of additive manufacturing is also due to the ability to work with different materials, which will be discussed in chapter 2.3.2.

2.3 3D PRINTING TECHNOLOGIES AND MATERIALS

2.3.1 3D-PRINTING TECHNOLOGIES

The main 3D printing techniques are Fused Deposition Modeling (FDM), Selective Laser Sintering (SLS), Selective Laser Melting (SLM), Three-Dimensional Printing (3DP), Direct Energy Deposition (DED), Stereolithography (SLA), and Digital Light Processing (DLP). The various mentioned techniques will be explained later, while chapter 2.4 will delve into vat photopolymerization, specifically focusing on DLP, the technique used in this thesis work.

FDM is a technique that involves the use of a continuous filament of thermoplastic polymer to 3D print layers of material. It is one of the most well-known and widely

used techniques in industrial as well as biomedical fields. The filament is heated by the nozzle to a semi-liquid state and then extruded onto the platform or over previously printed layers. The thermoplastic nature of the polymer filament is crucial for this method, as it allows the filament to melt during the printing process and then solidify again at room temperature after printing. Layer thickness, filament width and filament orientation are key processing parameters for this method. Figure 2.2 illustrates the operational process of FDM.

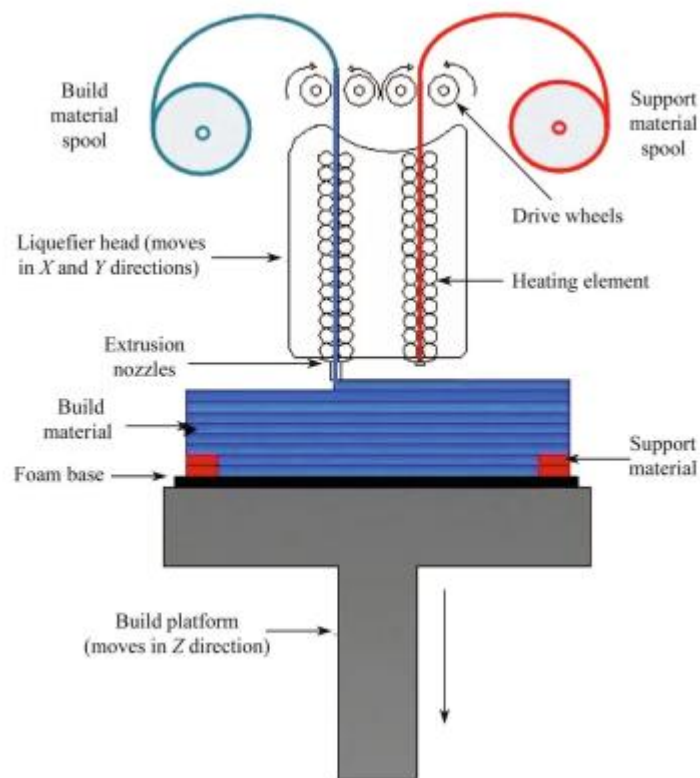


Figure 2.2 Schematic representation of the operation from the FDM [7]

This technique results in a final object that does not have strong mechanical properties. It has been found that layer-to-layer adhesion issues are the main cause of this mechanical weakness. Among its advantages, however, we can mention low cost, high speed, and process simplicity.

SLS, SLM, and 3DP are all processes that start with a bed of powder material to be printed. The difference among these three techniques lies in how the layers are formed: SLS and SLM utilize thermal energy, thus belonging to the Powder Bed Fusion category, while 3DP uses a binder and belongs to the Binder Jetting

category. In all three techniques, a roller spreads a new layer of powder over the previous layer to continue the printing process. Once the printing process is completed, excess powder is removed using vacuum, and additional processes such as sintering, infiltration, or applying a coating may be performed if necessary. Among the most crucial factors for the effectiveness of this method are particle size distribution and powder packing density, which determine the density of the printed part. SLS can be used with a variety of polymers, metals, and alloy powders, whereas SLM is limited to certain metals like steel and aluminum. SLS does not fully melt the powders, whereas SLM achieves complete powder fusion, resulting in superior mechanical properties. When a liquid binder is used, the method is referred to as 3DP. Important factors in this process include the chemistry and rheology of the binder, particle size and shape of the powder, deposition speed, interaction between powder and binder, and post-processing techniques. Printed parts exhibit higher porosity compared to parts produced through melting or sintering processes.

The main advantages of powder bed fusion techniques are fine resolution and high print quality, making them suitable for printing complex structures. Indeed, this method is widely used across various sectors for advanced applications such as tissue engineering scaffolds, aerospace, and electronics. A key advantage of this method is overcoming the challenge of support material removal, as the powder bed itself acts as the support. However, this process tends to be slow and associated with high costs.

Figure 2.3 illustrates the operational mechanism of SLS, SLM, and 3DP.

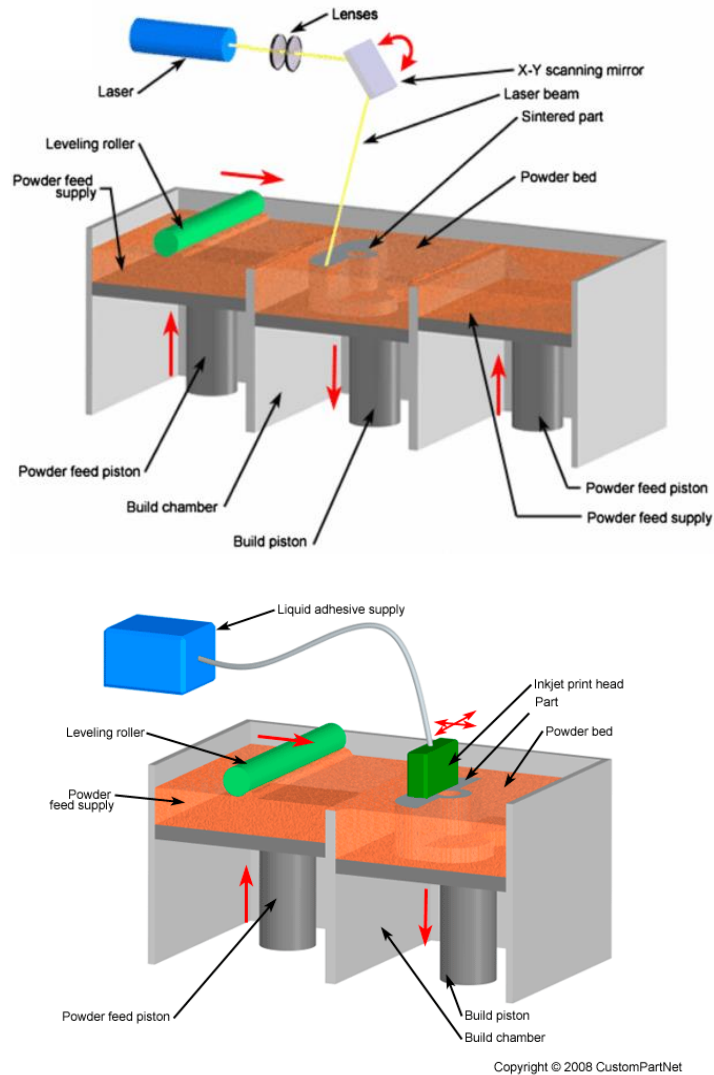


Figure 2.3 SLS and SLM process (above) and 3DP process (below).[8]

DED, or Direct Energy Deposition, is a technique primarily used for processing high-performance superalloys. This method utilizes an energy source such as a laser or electron beam, which is focused directly onto a small region of the substrate. During the process, a base material is simultaneously deposited, which can be in the form of powder or wire. The material is deposited and melted into the molten substrate and solidifies after the laser beam moves. This method allows deposition on multiple axes and simultaneous deposition of multiple materials. However, it offers lower precision and quality compared to SLM and SLS, resulting in the creation of less complex geometries. For this reason, DED is used for manufacturing large components with low complexity. DED reduces production time and costs while providing excellent mechanical properties and controlled microstructure. Figure 2.4 illustrates the operational diagram of DED.

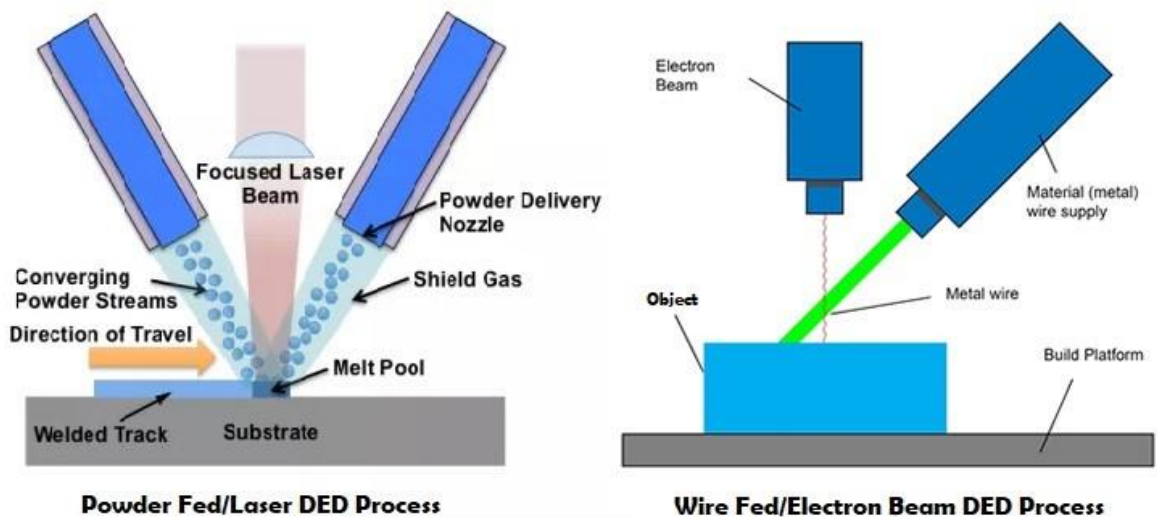


Figure 2.4 Laser DED process (left) e Electron Beam DED process (right)

The last two techniques mentioned among the most important are SLA (Stereolithography) and DLP (Digital Light Processing). They are vat photopolymerization techniques, utilizing a light source (UV or visible) to trigger the polymerization of a liquid resin contained in a vat. These two printing techniques will be described in more detail in section 2.4.1

2.3.2 3D- PRINTING MATERIALS

The growth of 3D printing, in addition to the variety of available technologies, is also attributed to the continuous discovery of new materials.

Among materials, metals and alloys are notable examples. Additive manufacturing of metals is showing promising growth. Typically, the 3D printing process for metals involves melting the metal feedstock (either powder or wire) using an energy source such as a laser or electron beam. The melted material is deposited layer by layer until a solid part is formed. The most commonly used techniques for printing metal materials are powder bed fusion (PBF) and direct energy deposition (DED). However, there are also other recently developed techniques such as binder jetting, cold spray, friction welding, and direct metal writing. These processes can achieve higher precision or speed. Titanium and its alloys, steel alloys, certain aluminum alloys, nickel alloys and some cobalt and magnesium-based alloys have been optimized for additive manufacturing (AM). 3D printing of these materials has

garnered increasing interest because conventional manufacturing methods are often associated with high processing costs. Therefore, AM can offer significant economic advantages by enabling the production of highly complex structures with lower costs and less waste. Titanium and Ti6Al4V, in particular, have been extensively studied and are currently used for applications in aerospace and biomedical sectors. Regarding aluminum alloys, only a few are used in additive manufacturing (AM) for several reasons. Compared to titanium alloys, processing aluminum alloys with conventional techniques is simpler and less costly, which reduces interest in their use in AM. Additionally, some high-performance aluminum alloys are difficult to weld, and aluminum itself has high reflectivity for laser wavelengths commonly used in AM. A positive aspect is that aluminum has high thermal conductivity, which reduces internal thermal stresses and allows for faster AM processes. In the biomedical field, cobalt-chromium alloys have been studied for biomedical and dental applications. [25], [29]

In addition to metals, polymers are also widely used in additive manufacturing (AM). Particularly, polymers are considered the most common materials in the 3D printing industry due to their versatility and ease of adoption across different 3D printing processes. They find applications in aerospace, automotive, sports, and medical industries. Polymers for additive manufacturing are available in the form of thermoplastic filaments, reactive monomers, resin, or powder. Using polymers in printers results in objects that may have suboptimal mechanical properties, prompting research efforts to address this issue. This research has led to the development of various methods and materials for producing advanced polymer composites with improved performance. Some of the advantages of manufacturing composites using 3D printing include the ability to customize geometry with high precision. Photopolymer resins are activated by UV light in stereolithographic 3D printing and begin to polymerize. However, the thermo-mechanical properties of photopolymers still need improvement. Among SLS polymers, there are polystyrene, polyamides, and thermoplastic elastomers. Systems based on photopolymers offer accuracy, thin layers, and high precision. Further developments in new resins have led to improved mechanical strength and temperature resistance. Currently, composite blends based on polylactic acid, a thermoplastic polymer, are used for 3D printed scaffolds in tissue engineering applications. For the

manufacturing of polymers and composites, various 3D printing techniques can be utilized: stereolithography, SLS (Selective Laser Sintering), FDM (Fused Deposition Modeling), 3D bioprinting, and inkjet printing. FDM is most commonly used for fabricating polymer composites and thermoplastics with low melting points. [30]

Finally, 3D printing techniques can also utilize ceramics. Additive manufacturing (AM) has become an essential method for producing advanced ceramics used in tissue engineering, such as creating scaffolds for bones and teeth. Despite the printing accuracy, challenges such as layer-by-layer production and a limited selection of materials are prominent in 3D printing ceramics. Additionally, the high cost and lengthy post-processing time required for sintering ceramic parts to achieve the desired shape have made 3D printing of complex shapes increasingly appealing.

The use of 3D printing has enabled the production of ceramic scaffolds for tissue engineering in a more cost-effective and faster manner compared to traditional methods like casting and sintering. In addition, the use of 3D printing allows for greater control over the porosity of ceramic structures. The main 3D printing methods for ceramics include inkjet printing, powder bed fusion, extrusion, and stereolithography. Inkjet printing is considered the primary method for producing dense ceramic samples that may not require post-processing. Selective laser sintering (SLS) of ceramic powders is also a common method for 3D printing ceramic materials. However, the thermal shock from heating for fusion and rapid cooling to room temperature can lead to cracking in ceramic parts. [31], [32]

2.4 PHOTOPOLYMERIZATION FUNDAMENTALS AND LIGHT-INDUCED 3D PRINTABLE FORMULATIONS

Photopolymerization is an effective method for crosslinking polymer chains covalently. Polymers that undergo free radical polymerization are modified with functional groups (acrylates). This polymerization reaction occurs in the presence of a photoinitiator and exposure to light, transforming the material from a fluid to a solid state under physiological conditions. The modulation of light intensity and wavelength ensures easy control over the polymerization rate, while exposure time adjusts the degree of crosslinking. In photopolymerization, the initial material is converted into insoluble polymers through irradiation with UV or visible light. UV light

is the most common activation source in photopolymerization, although compared to visible light, it raises concerns regarding user protection. Photopolymerization, particularly through UV irradiation, offers clear advantages such as rapid curing, solvent-free formulations, and lower energy consumption compared to thermal polymerization techniques. This is because UV curing operates at lower temperatures. [33]

The mechanism by which the starting material is converted into insoluble polymers can be of two types: radical mechanism and ionic mechanism.

1. **Radical Mechanism:** The reactive species is a free radical that initiates the reaction through propagation. This process can be divided into three main phases: initiation, propagation, and termination. During the initiation phase, light activates the photoinitiator, generating a reactive species, a radical. In the propagation phase, radicals react with monomers to form monomeric radicals, which in turn react with other monomers, leading to a chain reaction. In the termination phase, the reaction stops. Termination can occur when two growing chains react, and radicals become inactive. Termination can also occur in the presence of impurities, where the impurity can react with active groups, terminating chain growth. [34]

2. **Ionic Mechanism:** The reactive species in this case is an ion. Ionic photopolymerization offers several advantages compared to radical photopolymerization. Cationic polymerization is not inhibited by the presence of molecular oxygen and has minimal sensitivity to water. Additionally, the shrinkage of polymers polymerized via the ionic mechanism is lower compared to that observed in free radical photopolymerization. Despite these advantages, cationic photopolymerization is less common than radical photopolymerization because it tends to be slower.

In cationic photopolymerization, the initiation phase is typically carried out using onium salts (iodonium, sulfonium, alkoxyppyridinium), which absorb UV light and generate reactive cations. Similarly, anionic photoinitiators convert light energy into the formation of reactive anions, which add to the double bond of a monomer, transforming it into a propagating radical. Light-induced anionic polymerization is less represented in literature compared to cationic or radical polymerization.

Termination in ionic polymerization differs from radical polymerization because the reaction between similar ions is not possible. In this case, termination occurs when the chain reacts with impurities or other specifically added reagents through a disproportionation process.[35]

To ensure photopolymerization occurs, a photocurable solution with specific elements is necessary. A typical composition consists of a photoinitiator, monomer or a mixture of monomers, and possibly additives and fillers. Photoinitiators are compounds that decompose in the presence of UV, visible, and occasionally IR light, forming active species that initiate polymerization. The type and concentration of photoinitiator, irradiation time, temperature, intensity, and wavelength of the initial light all influence the reaction rate. Photoinitiators can be classified as type I (cleavable) and type II (hydrogen abstractors). The figure number shows the two types of photoinitiators. Type I initiators are more efficient than type II, but they produce more by-products. The properties of the photoinitiator are crucial for the success of photo-induced polymerization, significantly impacting the critical phase of reaction initiation. [36]

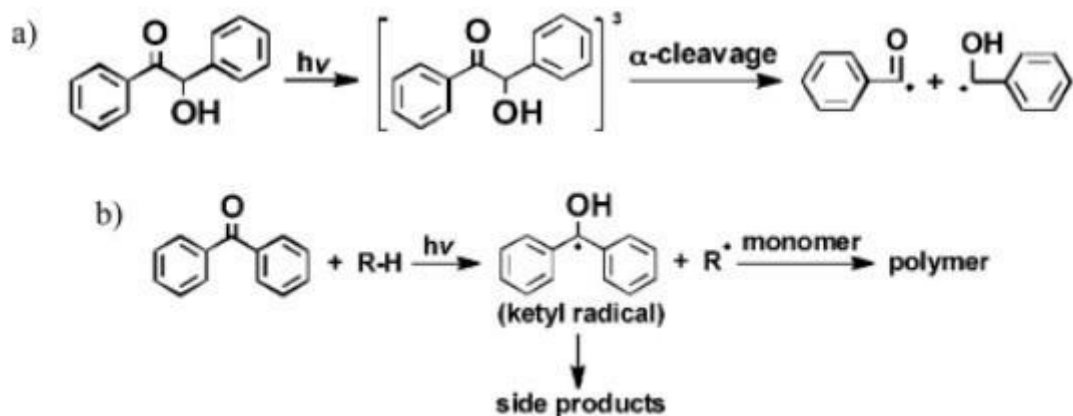


Figure 2.5 Photoinitiator mechanism: (a) Type I and (b) Type II [12]

2.4.1 3D VAT PHOTOPOLYMERIZATION: SLA AND DLP

Printing techniques based on photopolymerization can also be called vat photopolymerization. This term is used when the liquid precursor is contained in a vat. This type of process stands out as one of the most extensively studied printing methods due to its high printing speed and ability to produce high-resolution

structures. The vat utilizes monomers or oligomers of a liquid resin that polymerize when exposed to a light source of a specific wavelength. There are several variants of vat photopolymerization; historically, the first developed was stereolithography (figure 2.6), which uses a UV laser beam that travels along a programmed path, polymerizing the resin it that irradiates. Consequently, the laser must move and trace the entire volume of the printed object pixel by pixel. For this reason, stereolithography is a relatively slow method. [37]

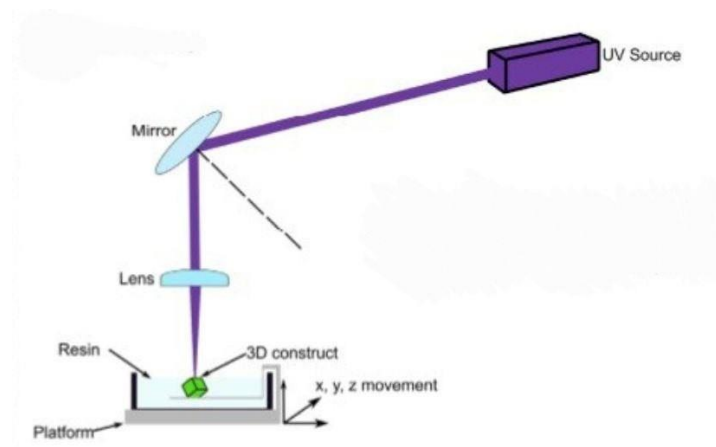


Figure 2.6 Stereolithography (SLA)

The vat techniques that use a digital light projector, such as DLP (figure 2.7), expose an entire layer of resin to light at once, masking areas that do not need to be polymerized. This makes DLP faster than SLA. [33]

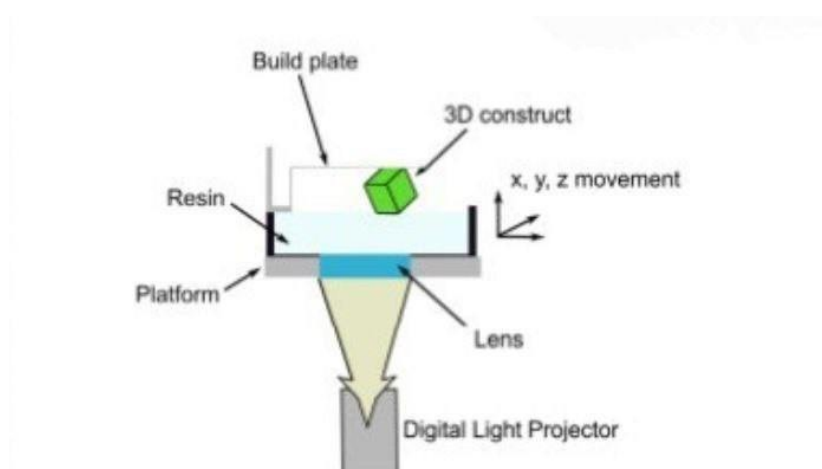


Figure 2.7 Digital light projector (DLP)

2.5 BIOMEDICAL CONSTRAINTS OF VAT 3D PRINTED DEVICES

Traditional methods have long been used to manufacture biomedical devices. However, the human body is composed of complex structures, and current production technologies are limited in material selection and manufacturing capabilities, failing to meet the requirements for producing bioinspired complex architectures and structures. It is in the perspective of wanting to create these types of structures that additive manufacturing finds its place. Specifically, thanks to its exceptional manufacturing capabilities, 3D printing processes prove to be a valuable tool in the biomedical field.

Vat photopolymerization was among the first 3D printing techniques proposed and is particularly relevant in the biomedical field because it can produce complex structures with high resolution. In addition to achieving complex and biomimetic structures, it is essential to consider the sensitivity of cells to various factors. Cells are sensitive to the environment in which they are cultured, and their behavior can be influenced by the properties of surrounding materials. Alongside the mechanical and physical properties of the chosen materials, it is crucial to consider biocompatibility as well. This represents one of the primary challenges in using VAT for 3D printing materials intended for the human body. For a 3D printed material to be biocompatible, it must meet several conditions: in addition to being printable, it must possess suitable mechanical properties, must not release toxic substances that can damage or kill cells, exhibit a controlled degradation process and not produce toxic by-products. Typical photosensitive resins contain acrylates or methacrylates as monomers and photoinitiators that can be toxic to cells. Therefore, currently, the study of new biocompatible materials for vat printing is gaining increasing interest. In addition to the presence of monomers and photoinitiators, the polymer blend often requires the use of other additives to modulate the properties of the final material and the behavior of the liquid resin during printing. It is essential that these additives are non-toxic to cells.

The use of 3D printed materials using vat photopolymerization in a biomedical context poses a specific set of challenges regarding both toxicity and desired properties of the final material. Although the polymerized material itself may be non-toxic, unreacted monomers and the initiator generally are. For this reason, the printing process must be followed by thorough washing using solvents such as

ethanol or isopropanol. However, this step can affect the mechanical properties of the 3D printed material, necessitating an additional post-curing phase where the printed object is exposed again to UV light to ensure complete polymerization and cross-linking formation. Figure number 2.8 illustrates the process of photocuring and polymerization that occurs during printing. [37], [38], [39], [40], [41]

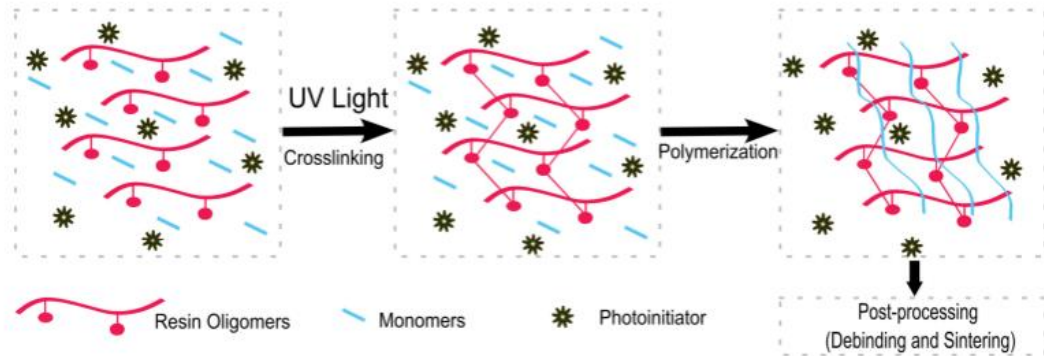


Figure 2.8 Process of photocrosslinking and polymerization before and during 3D printing process [37]

CHAPTER 3: MATERIALS AND METHODS

In the following chapter, the materials and methods used for the preparation of the samples and the techniques used to characterize the material will be analyzed.

3.1 MATERIALS

Based on previous researches, for the fabrication of the device, two different formulations were synthesized. The functional monomers selected for the production of the two resins are poly(ethylene glycol) diacrylate (PEGDA) and TEGORad.

Poly(ethyleneglycol)diacrilate is a photopolymerizable compound with good printability. The presence of acrylate groups in its chemical structure (Figure 3.2) allows for free radical polymerization. It is available in different molecular weights, and depending on the chosen weight, a specific cross-linking density can be achieved. In this thesis work, PEGDA 250 was selected, which is relatively hydrophobic and biocompatible even after the printing process. Fare clic qui per immettere testo. [42]

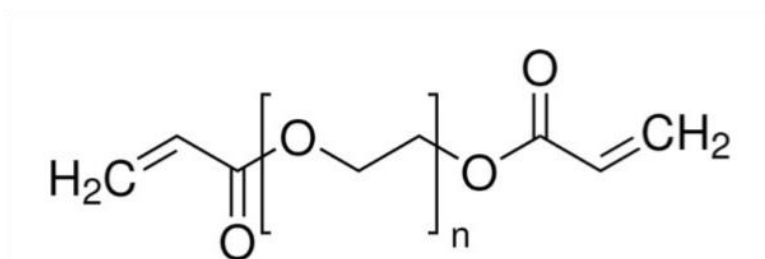


Figure 3.2 Chemical structures of poly(ethyleneglycol)diacrilate 250 (PEGDA 250) [43]

TEGORad 2800 (Figure 3.3) is an acrylate polydimethylsiloxane copolymer supplied by Evonik Industries AG (Essen, Germany). It exhibits the same characteristics of Polydimethylsiloxane (PDMS), which is the most commonly used material for microfluidic device fabrication but surpasses its limitations. In choosing the resin, the need for optical transparency, biocompatibility and the absence of cytotoxic effects played an important role. Several tests have shown that cell viability and proliferation were supported on this material.[44]

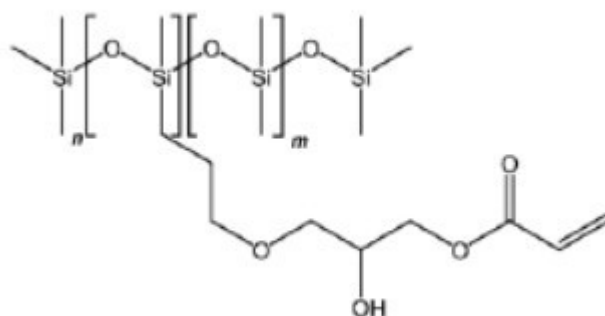


Figure 3.3. Chemical structures of TEGORad 2800

The selection of the components for the two formulations was based on the characteristics required for the structure to be printed. Specifically, PEGDA, which proved to be adhesive to cells, was used to create the base of the device and the wells' base. The following components were used for the PEGDA formulation and base:

- Phenylbis(2,4,6-trimethylbenzoyl)phosphine oxide (BAPO) was used as the photoinitiator;
- Pentaerythritol tetrakis (3,5-di-tert-butyl-4-hydroxyhydrocinnamate) (PT) was used as the radical scavenger.

Both components were found to be soluble in PEGDA 250, making the addition of solvents unnecessary. The chemical structures of the aforementioned reagents are shown in Figures 3.4.

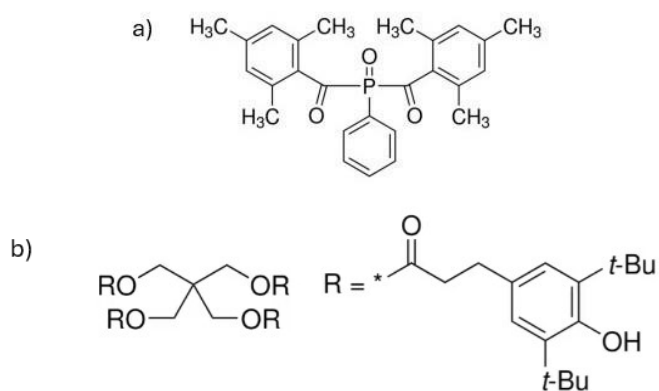


Figure 3.4 Chemical structures of a) BAPO and b) PT [43]

TEGORad, on the other hand, was used to print the walls of the wells and the microfluidic part of the device. Due to its lack of high rigidity, achieving such complex structures required the addition of dyes to allow for greater control over light penetration into the resin along the Z-axis. The components used are:

- Phenylbis(2,4,6-trimethylbenzoyl)phosphine oxide (BAPO) was used as the photoinitiator, but it was solubilized in another photoinitiator: 2-Hydroxy-2-methylpropiophenone (Omnirad 1173);
- Several dyes were used, including Dansyl Chloride, Methyl Red, Tartrazine, Coumarin 6, and Disperse Red 1 methacrylate (DR1-MA). All these dyes required solubilization in methyl methacrylate (MMA).

In Figure 3.5, the chemical formulas of all components used in the formulation based on TEGORad are shown.

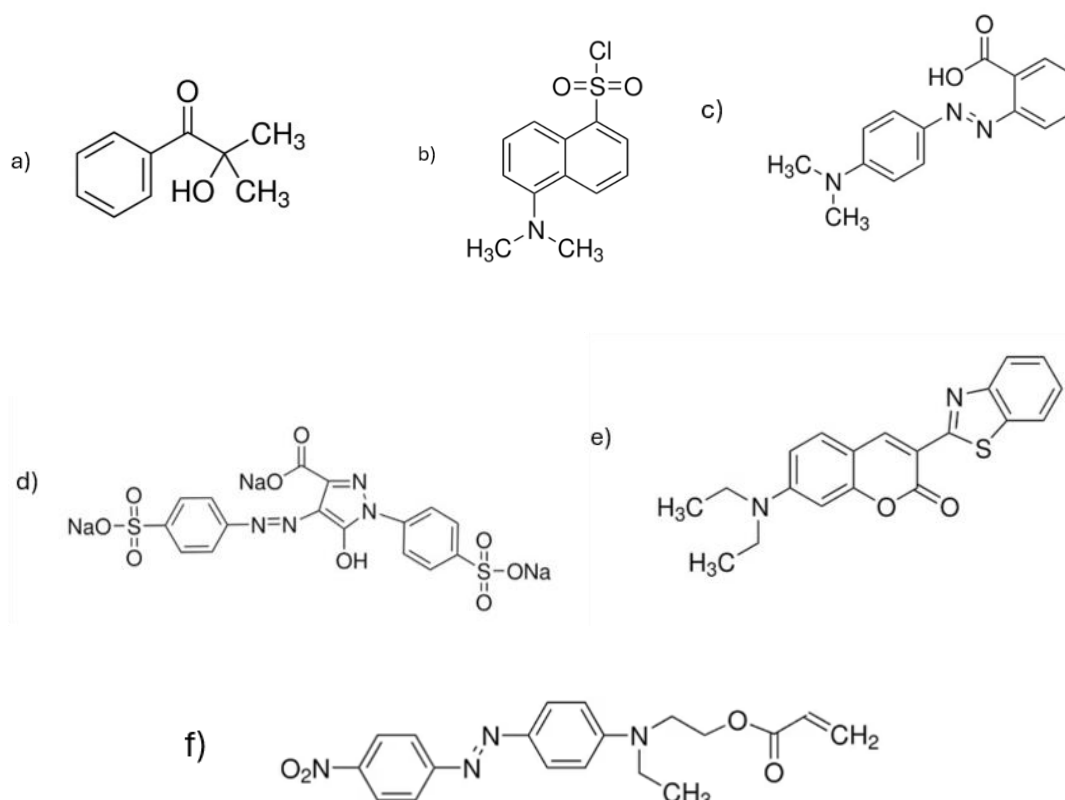


Figure 3.5 Chemical structures of a) Omnirad 1173 b) Dansyl Chloride c) Methyl Red d) Tartrazine e) Coumarin 6 and f) DR1-MA [43]

The choice of photoinitiators, Phenylbis(2,4,6-trimethylbenzoyl)phosphine oxide (BAPO) and 2-Hydroxy-2-methylpropiophenone (Omnirad 1173) was based on their adequate absorption of the emission wavelength of the selected 3D printer (405 nm).

All the mentioned components, except for TEGORad, were purchased from Merck.

3.2 DLP 3D PRINTER

For the 3D printing phase, the Pico 2 HD DLP-3D printer manufactured by Asiga and shown in Figure 3.2 was used. It is a DLP-type printer with a light source emitting at a wavelength of 405 nm, a nominal resolution in the XY plane of 50 μm and a minimum control along the z-axis of 1 μm .



Figure 3.1 Asiga Pico 2 HD DLP-3D [45]

The control of this printer is managed through a specific program, Asiga Composer, which allows for sending the files of the objects to be printed to the printer. These files can be of types STL, SLC, PLY and STM. Before sending the file to the printer, this program allows for the definition of various printing parameters. Typically, the main parameters to be defined are:

- Layer thickness;
- Light intensity;
- Exposure time.

Other parameters can also be adjusted, such as the platform movement speed during the approach and retraction phases or the waiting times between the different printing phases. When defining the parameters, various ranges can be set, and a distinction can be made between Burn-In and Range. Burn-In represents the initial layers, which usually have a longer exposure time to promote the adhesion of the curing material to the platform. The parameters chosen for the printing of the plate will be described in paragraph 4.2

3.3 PREPARATION OF FORMULATIONS

3.3.1 PEGDA

For preparing the PEGDA-based formulation, no solubilization of components was necessary. A dark Falcon was used to prevent polymerization of the formulation due to visible light. The resulting solution was then sonicated for 5 minutes to achieve homogeneity. Once sonication was complete, the resin was ready for the printing process.

3.3.2 TEGORAD

For the preparation of the TEGORad-based formulation, the process began with solubilizing components that were initially insoluble in the resin. Specifically, BAPO was solubilized in Omnirad 1173, while the dyes were solubilized in MMA (methyl methacrylate).

In order to print most of the device using the TEGORad-based formulation, larger quantities of the formulation were prepared compared to the PEGDA-based formulation. For this reason, the preparation was conducted in larger, transparent plastic containers, which were covered with foil to prevent resin polymerization from light exposure. The solution was initially placed on a magnetic stirrer for 15 minutes, and then sonicated for 5 minutes at 35°C. Once the sonication process was completed, the resin was ready for the printing process.

3.4 WASHING PROTOCOL AND STERILIZATION PROTOCOL

At the end of the printing process, the obtained samples may contain unpolymerized material within them. Since the 3D printed plates are intended for use in a bio-compatible context, in contact with cells, it was necessary to establish a washing

protocol. This step is crucial because even though starting materials may be non-toxic to cells, unreacted reagents could potentially pose a risk.

To define this washing protocol, solvents such as acetone, isopropanol and ethanol were used, as they are found to effectively remove residual uncured material while being compatible with biological applications.

Once the washing protocol is completed, the obtained objects still cannot be used directly in contact with cells. Therefore, it was necessary to define a sterilization protocol as well. For sterilization, the 3D printed plates were placed in a Phosphate Buffered Saline (PBS) bath and subsequently exposed to UV light in a biological safety hood for 30 minutes.

This sterilization process aids in the removal of any residual contaminants on the surface of printed objects, making them suitable for use in biological applications where sterility is critical.

3.5 CHARACTERIZATION METHODS

Once the smart plate was obtained, the following characterizations were performed:

- Fluidic assessment of the system perfusion;
- UV/Visible Spectroscopy to define washing protocol and to evaluate absorption and fluorescence of the system;
- Conditioned medium cell culture to evaluate the release of cytotoxicity compounds:
- Cell Viability and Proliferation of cells seeded on the system.

3.5.1 FLUIDICS ASSESMENT OF THE SYSTEM PERFUSION

To enable the investigation of the behavior of the system in a dynamic environment, before testing the devices, flux simulations were performed using 2 different software, Solidworks and Comsol. Solidworks was used to create the CAD model and fill the model with a fluid as shown in Figure 3.6. This was necessary because, in fact, before starting the peristaltic pump to recirculate the culture medium and/or other solutions, the cells on the bases of the wells are covered with culture medium. When conducting such simulations, it is crucial to represent all the real initial conditions.

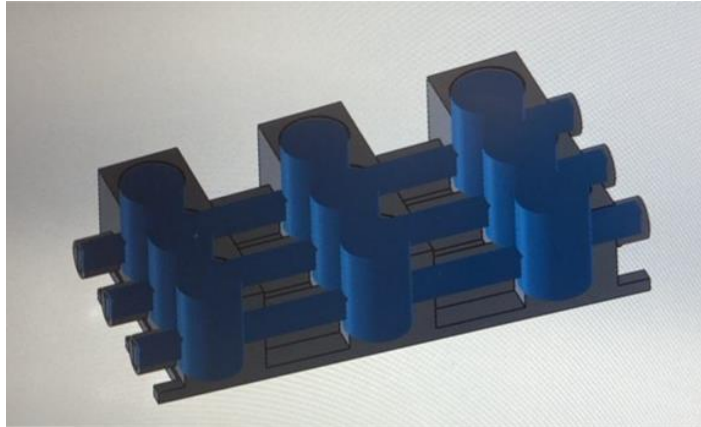


Figure 3.6 Wells filled with fluid.

After creating the CAD and generating fluid volumes in all the wells, the file was imported in STL format into Comsol, which allowed the various flow rates permitted by the chosen peristaltic pump (i.e. 50 $\mu\text{l}/\text{min}$ - 500 $\mu\text{l}/\text{min}$). Before starting the simulation, various parameters were defined, such as the stiffness of the two materials constituting the smart plate, the hydrophilicity of the materials and the viscosity of the culture medium.

The selected flow rates are as follows:

- a. 50 $\mu\text{l}/\text{min}$
- b. 100 $\mu\text{l}/\text{min}$
- c. 200 $\mu\text{l}/\text{min}$
- d. 300 $\mu\text{l}/\text{min}$
- e. 400 $\mu\text{l}/\text{min}$
- f. 500 $\mu\text{l}/\text{min}$

The main parameters studied were the flow rate (m^3/s), the pressure (Pa) that develops in the inlet and outlet sections of the flow and on the walls of the wells, and the velocity (m/s) at the inlet, outlet and that which occurs as the flow passes through the wells. The latter is critical to understand whether the velocity that develops at the bottom of the well may be detrimental to the cells themselves. Using the simulations, the maximum values of pressure and velocity and the respective locations in the device where these occur were identified.

After the various simulations had been carried out, experimental tests were performed using a 2-head peristaltic pump. In order to visualize the flow, a 1:50 solution of H₂O and Disperse Blue, a dye purchased from Aldrich Chemical Co, was created. The pump chosen is LiveFlow from IVTech, shown in Figure 3.7.



Figure 3.7 LiveFlow Peristaltic Pump[46]

3.5.2 UV/VISIBLE SPECTROSCOPY

UV/Visible spectroscopy is an investigative technique that can be employed for the evaluation of absorption or transmission of radiation with wavelengths in the UV/Visible range.

For the characterization of the smart plate, UV/Visible spectroscopy was used to study various aspects, employing the Synergy HTX plate reader manufactured by BioTek (Figure 3.9). First, this investigative technique was employed to define the washing protocol of the smart plate by studying the absorbance of different washing solutions. This was done to determine if the material, once printed and washed, continued to release substances, like dye or unreacted resin. Absorbance tests were set between 300 and 700 nm with intervals of 1 nm.

To be able to perform cellular assays and/or cellular staining, the employed system does not have to interfere with the generated signals. For this reason, UV/Visible spectroscopy was also used to study and compare the absorbance of standard laboratory 96-well plates (purchased from Greiner Bio-One) and the smart plate obtained through 3D printing, with absorbance spectra evaluated set between 300 nm and 700 nm at intervals of 1 nm. To perform the measurement, the lid of a 96-well multiwell was used and a holder for the smart plate was designed with Solidworks CAD and then fabricated in PMMA through milling (Figure 3.8)

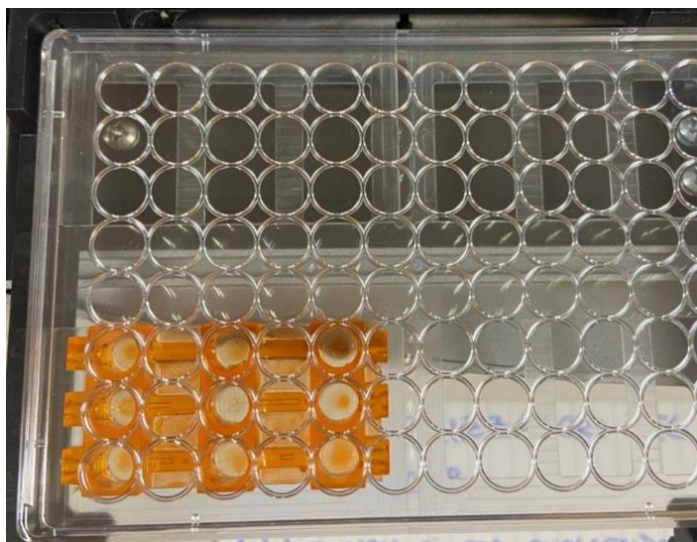


Figure 3.8 Lid and support in PMMA to perform the measurement

This type of analysis is based on the Lambert-Beer law, which models the attenuation of monochromatic light radiation as it passes through a material.

$$\log\left(\frac{I_0}{I}\right) = A = \epsilon lc$$

The following formula represents the Lambert-Beer law, where:

- I_0 = intensity of the incident monochromatic beam;
- I = intensity of transmitted monochromatic beam;
- A = absorbance;
- ϵ = molar attenuation coefficient characteristic of the species causing the radiation absorption;
- c = uniform concentration of the species;
- l = optical path length traversed by radiation.

From this type of analysis, a graph of absorbance (A) as a function of the wavelength (λ) of the attenuated radiation is obtained. If the wave passes through unaltered, the absorbance will be zero. In the presence of attenuations, peaks can be observed in the spectrum at the specific wavelength. [47]

Finally, the Synergy HTX plate reader was also used to perform fluorimetric analyses. Fluorimetry is an investigative technique that allows for the evaluation of the emissive properties of a material by measuring the light emission once it is excited at a specific wavelength. To assess the fluorescence of the fabricated smart

plate, the following excitation/emission wavelength were tested and compared with the commercial 96-well plate:

- 360/460 nm;
- 485/528 nm;
- 530/590 nm.



Figure 3.9 Biotek Synergy HTX Multimode Reader [48]

3.5.3 CYTOTOXICITY

Cytotoxicity tests are essential to evaluate the cytocompatibility of materials that come into contact with cells. These tests determine whether a material release substance that could be toxic for the cells, causing damage or cell death. The method chosen for cytotoxicity study in this Thesis works is the conditioned medium test. In this test, the smart plate was sterilized through a 10 minutes sonicating bath in ethanol 70%, overnight incubation in sterile ddH₂O and 30 min UV light for each side under examination is incubated in a cell culture medium for a specified period (i.e. over-weekend). Subsequently, the medium is collected and used to culture cell. In our case, the conditioned medium test was performed on 3 different cell types, including two cell lines and one primary cell type. All the cells lines were cultured in a cell culture incubator, at 37°C, 95% humidity, 5% CO₂. Specifically, we worked with:

- Human fibroblast (HFF1) provided by ATCC;
- Human keratinocytes (HaCaT) provide by Antibody Research Corporation;
- Endothelial cells (EC) kindly gifted by IRCCS Candiolo Institute.

Based on the cells used, different culture media were employed:

- For HaCaT and HFF1 cells: DMEM GlutaMAX supplemented with 15% Fetal Bovine Serum, 1% penicillin-streptomycin, 1% L-glutamine, 1% sodium pyruvate;
- For EC cells: a 1:1 mixture of DMEM GlutaMAX (supplemented as previously described) and F12K supplemented with 10% Fetal Bovine Serum, 1% penicillin-streptomycin, 0.01 mg/ml Heparin and brain extract supplement.

HaCaT, HFF1 and EC were detached from Petri dishes using Trypsin 2.5 X and seeded onto a 96-well plate at a concentration of 10 000 cells/well in the specific cell culture medium that had been incubated overnight with the smart plate and filtrated through a 0.22 um PES filter (200 µl per well). The cells were then incubated at 37°C with 5% CO₂ for 24 hours. After 24 hours, a cell viability analysis was performed. The culture medium in which the cells were grown was collected, and a solution of MTT (3-(4,5-Dimethylthiazol-2-yl)-2,5-Diphenyltetrazolium Bromide) at 0.5 mg/ml was prepared in culture medium and supplied to the cell (200 µl per well). MTT is used to assess cell viability as a function of redox potential. Viable cells were able to convert the water-soluble MTT to an insoluble purple formazan in a 2h incubation time at 37°C, 95% humidity, 5% CO₂. The formazan is then solubilized by discarding the MTT solution and adding 200 µl of DMSO. Lastly, its concentration was determined by optical density.

Using the Synergy HTX plate reader, measuring absorbance at specific wavelengths: 570 nm to read MTT and 650 nm to subtract the polystyrene signal of the plate. The signal from cells cultured in normal medium was used as a control. The same procedure was repeated on cells cultured for 72 hours in conditioned medium. Differences between groups were analyzed using two-way ANOVA.

3.5.4 ASSESMENT OF FEASIBILITY OF THE PLATE TO ANALYZE CELLULAR ASSAYS

As previously assessed in the conditioned medium experiment, MTT is one of the most broadly used assays to evaluate cell metabolism. As the smart plate will be used to culture cells, it is important to be sure that the material properties (for example, the dye presence) do not affect the analysis of such assay. To do that, HFF-1 cells were cultured on a commercial cell culture treated polystyrene 96 well plate for 72h, in DMEM high glucose (gibco) or MEM low glucose (gibco) cell culture media (supplemented with 15% FBS, 2% L-glutamine, 1% penicillin-streptomycin

and 1% sodium pyruvate). The two cell culture media were selected to see a difference in metabolism between the two conditions and to be able to evaluate if these differences were detectable also using the smart plate. After the 72h of culture, cells were incubated with 0.5 mg/ml MTT solution (200 μ l) for 2 hours. After the incubation, MTT was removed and cells were resuspended in 200 μ l of DMSO. A first absorbance reading (at 570 nm and 650 nm as before) was performed in the polystyrene well plate. Then, the DMSO solution was moved in a smart plate and the absorbance was read again. The experiment was repeated twice.

3.5.5 CELL VIABILITY AND PROLIFERATION

To test cell viability and proliferation, colorimetric and fluorimetric assays were conducted. Human fibroblast (HFF1), human keratinocytes (HaCaT) and endothelial cells (EC) were seeded directly on the smart plate wells and cell viability was analysed after 24 and 74h. To assess cell viability and proliferation directly on the smart plate, 100 μ l of 0,15% w/v gelatin was applied to the bottom of the plate wells for 30 minutes and then aspirated to obtain an adhesive coating, exposing the RGD groups on the surface, which are responsible for cellular adhesion. HaCaT, HFF1 and EC cells were seeded at a concentration of 10 000 cells/well and cultured for 24 and 72h. Cell viability was assessed both using again MTT assay and using a live/dead assay involving calcein-AM and propidium iodide (PI). Calcein-AM is a dye that does not fluoresce until it enters a live cell, where it emits strong green fluorescence. On the other hand, propidium iodide is unable to enter live cells due to their intact membranes, but it can passively enter dead cells due to their increased membrane permeability. Propidium iodide emits strong red fluorescence upon binding to nucleic acids. To conduct this assay, work was performed under a biological safety hood in darkness because exposure to light could potentially quench the fluorescent components.

To perform this test, the culture medium in the wells was aspirated and replaced with a PBS solution containing 1 μ l of propidium iodide and 2 μ l of calcein per ml of PBS. To distinguish between live and dead cells, the plate was then incubated at 37°C for 15 minutes. After 15 minutes, the PBS solution was removed and fresh PBS was added. To observe the results, the Nikon CSU-X1 Spinning Disk System (Figure 3.10) was used.



Figure 3.10 Nikon CSU-X1 Spinning Disk System [49]

3.5.6 FIRST TRIALS OF PERFUSED 3D GeIMA HYDROGEL SCAFFOLDS

Gelatin methacryloyl (GelMA) was produced according to the method initially described by Van Den Bulcke et al. (**REF A. I. Van Den Bulcke, B. Bogdanov, N. De Rooze, E. H. Schacht, M. Cornelissen, H. Berghmans, *Biomacromolecules* 2000, 1, 31.**) In summary, type B gelatin sourced from bovine skin (Sigma Aldrich) was dissolved in Dulbecco's Phosphate Buffered Saline (DPBS, Sigma) at a concentration of 10% w/v, heated at 50°C. To introduce methacrylate groups, 8 ml of Methacrylic Anhydride (MA, Sigma) was gradually incorporated. The reaction lasted for 2h before being interrupted by dilution with an equal volume of DPBS . The resulting solution underwent a week-long dialysis process against double-distilled water (dd-H₂O) using a cellulose membrane with a molecular weight cutoff of 12–14 kDa (Sigma) at 40°C, aimed at eliminating any remaining unreacted MA. Finally, GelMA was subjected to freeze-drying and stored for further use.

To test the possibility of using the smart plate to culture 3D hydrogel-based perfused scaffolds, GelMA formulation was obtained by dissolving the synthesized GelMA at 10% w/v concentration in DMEM (Gibco) cell culture medium, previously combined with lithium phenyl-2,4,6-trimethylbenzoylphosphinate (LAP) as photoinitiator at a

concentration of 2.5 mg/ml. The solution were heated at 60°C for 1h and filtered through 0.22 µm PES membrane filters (Asimo) to sterilize. GelMA solution was pre-warmed at 37°C before pouring it in the smart plate. Smart plate channels were then temporary occluded with a stainless steel needle with a diameter of 0.7 mm . 300ul of GelMA were poured in each well of the smart plate and photocrosslinked thanks to UV light irradiation ($\lambda = 365 \text{ nm}$, Asiga® Flash Cure Box, $I = 10 \text{ mW cm}^{-2}$) for 1 min. At this point, the needle was carefully removed and manual perfusion of ddH₂O and Disperse Blue 1 was performed. After the perfusion, GelMA samples were removed, unraveling the formation of channels.

CHAPTER 4: RESULTS

This thesis aimed to develop a microfluidic device for cell culture and/or drug testing. To achieve this device, a CAD model was initially created and subsequently modified several times to ensure it could perform all its intended functions. Once the final CAD model was chosen, the device was characterized in terms of its chemical-physical properties and its biological performance. This chapter will present and analyze the results obtained from the experimental tests conducted.

4.1 SOLIDWORKS DESIGN

To create the device, the first step was to use dedicated software to develop a CAD model representing the geometry intended for printing. In this case, the CAD model was created using Solidworks. Aiming to produce a device compatible with existing laboratory analysis instruments, we sought to develop a CAD model that resembled the design of a standard laboratory plate (Figure 4.1). Unlike a regular polystyrene laboratory plate, the smart plate must also incorporate channels capable of allowing the flow of culture medium and/or other solvents and materials, such as drugs and soluble factors.

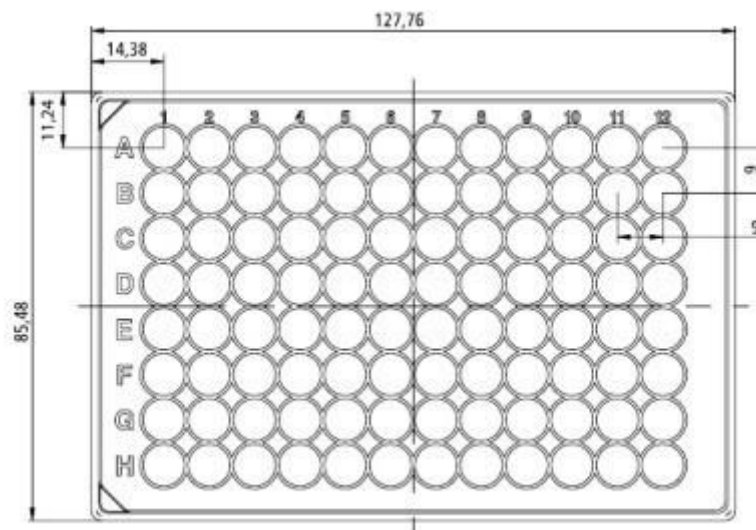


Figure 4.1 Multiwell design

The CAD model was based on a design studied and produced in a previous Thesi work. As shown in Figure 4.2, the smart plate features 9 wells and 3 parallel channels, each with its respective inlet and outlet. The decision to arrange 3 wells

in series and in parallel was made to allow for triplicate and parallel experiments within the same plate.

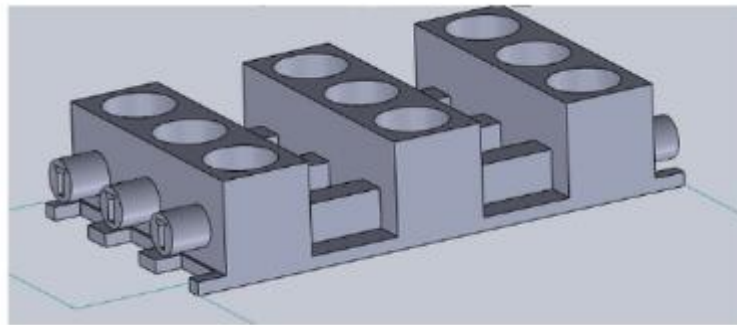


Figure 4.2 CAD di partenza per la realizzazione della piastra smart

However, anticipating some results, once the device was printed issues arose regarding the assembly of the tubes needed to connect the smart plate to a peristaltic pump, which is essential for conducting fluidic tests on the device. The previous CAD model featured inlets and outlets with 'Y'-shaped holes. This shape was initially chosen to facilitate the printing of the channels, considering the challenges encountered when printing with a material like TEGORad, which tended to collapse during the process. However, despite making it easier to create the holes and open channels, the 'Y' geometry was not compatible with any available tubing for subsequent flow tests. Therefore, it was necessary to modify the shape of the inlets and outlets to have circular holes with a diameter of 1 mm. This diameter was chosen based on the diameter of the tubes used with the pump selected for microfluidic tests. The final CAD model is shown in Figure 4.3.

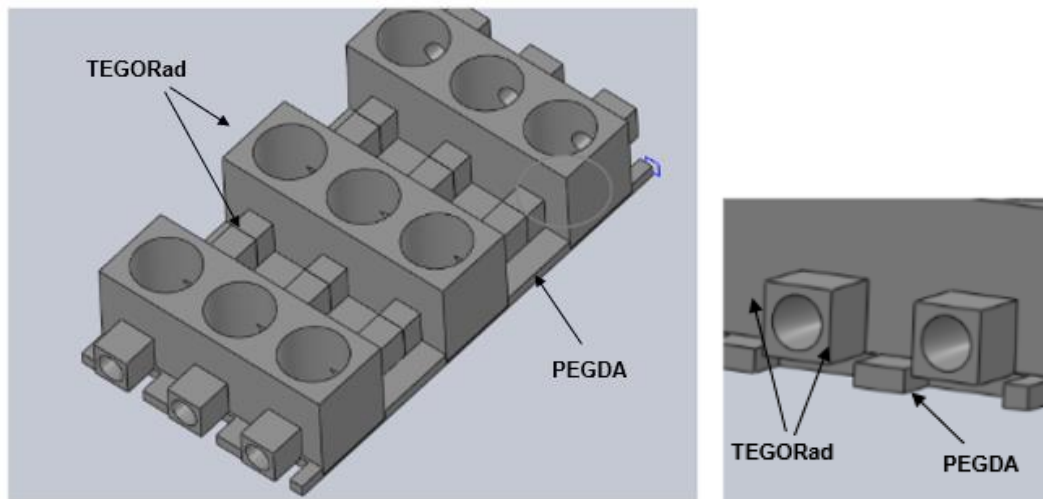


Figure 4.3 New CAD of the smart plate made with Solidwors and shape of the inlet and outlet holes (right)

Once the CAD model of the smart plate was created, a CAD model for the plate cover was also designed using the same software. The decision to create the cover was made for three main reasons:

1. To mimic the design of a standard laboratory plate, which typically includes a snap-on cover.
2. To use the smart plate in a biological setting, where maintaining sterility is a fundamental requirement.
3. To create a dynamic device, as the absence of a cover could cause the fluid to overflow from the wells due to the high resistance encountered when the fluid tries to enter the wells.

Figure 4.3 shows the CAD of the lid and the 3D prited smart plate and lid.

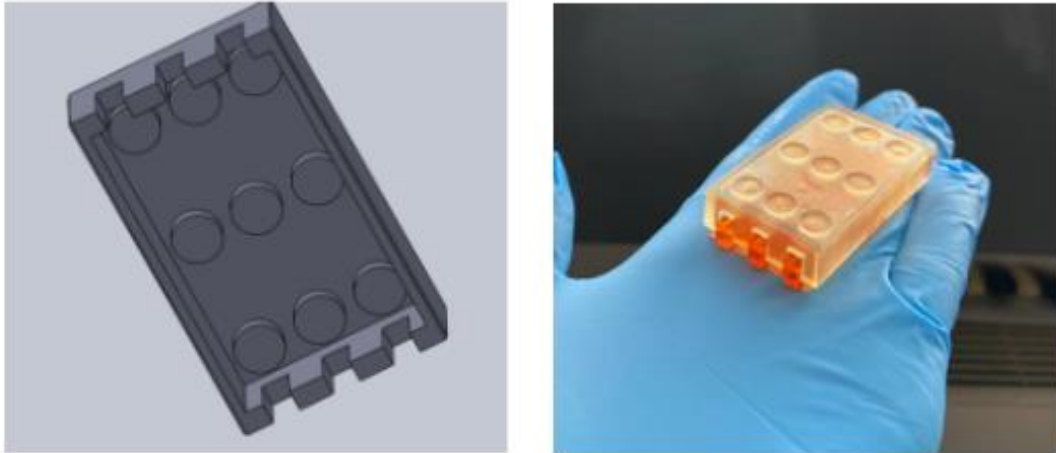


Figure 4.3 CAD of the smart plate lid (left) and 3D printed smart plate and lid (right)

4.2 FORMULATIONS

The need to have plate structures that promote cell adhesion and others that inhibit it without causing cytotoxic effects, as mentioned in Chapter 3.1, led to the development of a bimaterial plate. To create the device using a Digital Light Processing (DLP) printing process, it was necessary to develop formulations capable of reacting and polymerizing when exposed to light radiation. A typical photopolymer composition consists of different components:

- Photoinitiator: a monomer or a mixture of monomers that decomposes when exposed to light (UV, visible, and, more rarely, IR light), producing active species such as free radicals or cations, which initiate the polymerization process;
- Additives: elements that allow greater control over certain aspects of the printing process. In this thesis, dyes and a radical scavenger were used. The dyes enabled control of the light penetration depth into the resin, modulating the polymerization reaction more significantly along the Z-axis, while the radical scavenger allowed control of the reaction propagation in the plane transverse to the light (XY plane).

In particular, two different formulations were developed: one in which the functional monomer was poly(ethylene glycol) diacrylate 250 (PEGDA 250), and a second formulation in which the functional monomer was TEGORad 2800. The

choice of components for both formulations was based on formulations studied in a previous thesis projects.

4.2.1 PEGDA FORMULATION

The poly(ethylene glycol) diacrylate 250 (PEGDA 250)-based formulation, due to the known ability of PEGDA to promote cell adhesion, was used to print the base of the device and the bottom of the wells. As mentioned earlier, the starting point was formulations that had already been developed; in the case of the PEGDA-based formulation, we started with the formulation reported in Table 4.1.

Component	Name	%wt*
Monomer	PEGDA 250	
Photoinitiator	BAPO	1
Dye	Dansyl Chloride	0.1
Radical Scavenger	PT	0.1

* percentage by weight to resin

Table 4.1 Starting PEGDA-based formulation

Starting from this formulation, it was necessary to make some modifications due to the choice of the printing device. In fact, in the previous investigations, a DLP printer with a light source emitting at a wavelength of 385 nm (UV spectrum) was employed. Differently, in for this thesis the Asiga Pico 2 HD DLP-3D printer was used, which emits light at a wavelength of 405 nm (visible spectrum). Furthermore, in the envisaged work flow PEGDA should be printed only in simple geometries—specifically, the bottom rectangular structure. Consequently, it was decided to remove Dansyl Chloride from the formulation. To define the new formulation, printing tests were conducted to verify the feasibility of working without using a dye. The simplicity of the structures and the reduced number of layers to be printed allowed for defining the new formulation simply by removing Dansyl Chloride. Table 4.2 represents the final formulation used after this adjustment.

Component	Name	%wt*
Monomer	PEGDA 250	
Photoinitiator	BAPO	1

Radical Scavenger	PT	0.1
--------------------------	----	-----

* percentage by weight to resin

Table 4.2 PEGDA-based final formulation

The same formulation was used to make the plate lid.

4.2.2 TEGORad FORMULATION

The TEGORad-based formulation was used to create the walls of the wells and the microfluidic structures. This material was chosen because unlike PEGDA, TEGORad inhibits cell adhesion without inducing cytotoxic effects. Similar to the PEGDA-based formulation, this formulation was developed based on previous work. Table 4.3 shows the formulation from which we started for this purpose.

Component	Name	%wt*
Monomer	TEGORad 2800	
Photoinitiator	BAPO in Omnirad (1:4 solution)	0.8
Dye	Dansyl Chloride in MMA (1:50 solution)	0.075

* percentage by weight to resin

Table 4.3 TEGORad-based starting formulation

The definition of the new formulation was more problematic than the definition of the new PEGDA-based formulation. This was due to the complexity of the structures to be made and the properties of the chosen material. TEGORad, in fact, tends to collapse during the photopolymerization process, not allowing the desired geometry to be perfectly achieved. This aspect was the key point in defining the formulation, as the need to have to obtain microfluidic structures that would allow the flow of culture medium, drug or other soluble substances, resulted in the need to use a dye that would allow good control in polymerization along the Z axis.

As mentioned in Chapter 4.2.1, the choice of a different printing device necessitated the removal of components that do not absorb at the emission wavelength of the printer. Similarly, Dansyl Chloride was removed in this case, prompting consideration of alternative dyes for replacement.

Having to use the smart plate in a biological context and wanting to analyze cellular viability directly within the smart plate, it was decided to start with a dye that would allow for a transparent structure to observe activities inside the plate, including fluidics. The first dye chosen was Tartrazine, which met the transparency requirement but did not yield well-defined channels (Figure 4.4) capable of allowing the flow of culture medium, drugs, and other soluble substances. In Table 4.4, the formulation based on TEGORad with Tartrazine is shown.

Component	Name	%wt*
Monomer	TEGORad 2800	
Photoinitiator	BAPO in Omnirad (1:4 solution)	0.8
Dye	Tartrazine in MMA (1:50 solution)	0.85

* percentage by weight to resin

Table 4.4 TEGORad-based formulation with Tartrazine

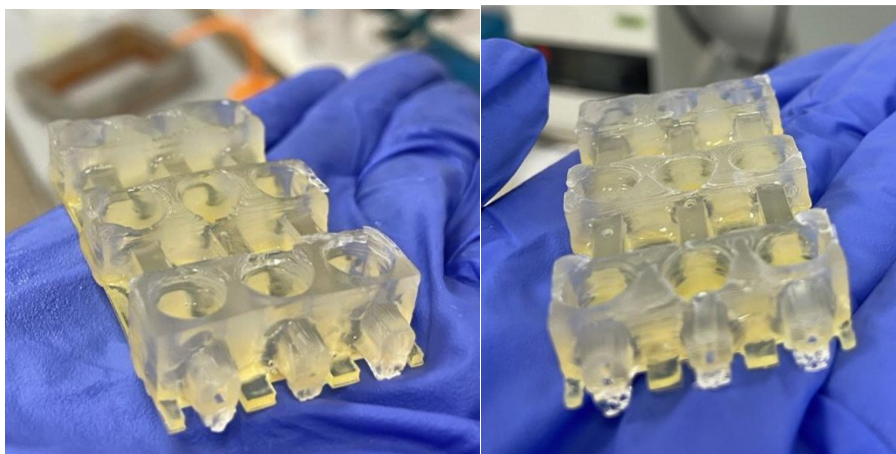


Figure 4.4 Smart plate with Tartazine

A second dye used was Coumarin 6. The use of this formulation, as shown in Table 4.5, allowed for well-defined devices, as depicted in Figure 4.5. However, despite the excellent definition, open channels capable of allowing flow could not be achieved.

Component	Name	%wt*
Monomer	TEGORad 2800	
Photoinitiator	BAPO in Omnirad (1:4 solution)	0.8
Dye	Coumarin 6 in MMA (1:50 solution)	0.85

* percentage by weight to resin

Table 4.5 TEGORad-based formulation with Coumarin 6

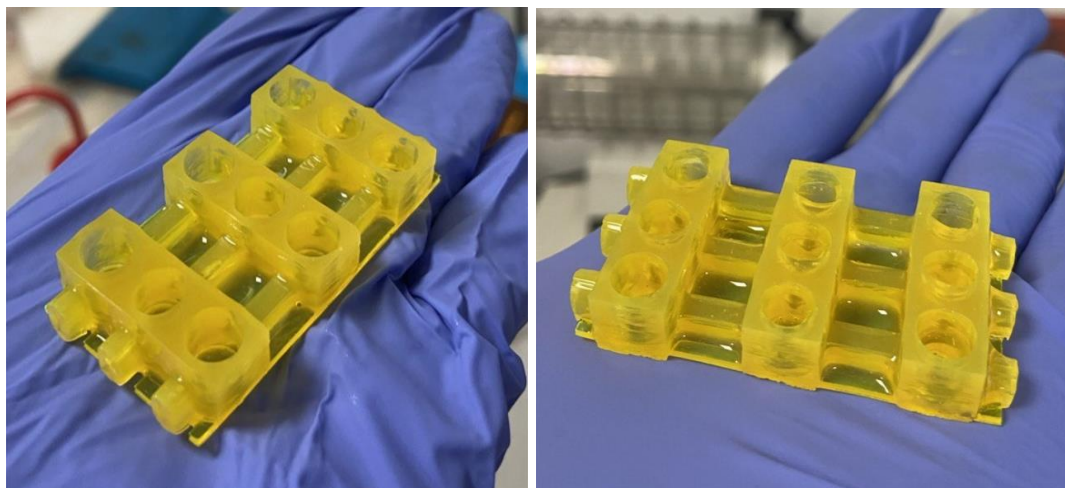


Figure 4.5 Smart plate with Coumarin 6

The first dye that allowed for a device to achieve not only good definition but also open channels capable of permitting flow was Methyl Red. Starting with a formulation containing a high quantity of dye (Table 4.6), the goal was to determine if this would assist in controlling polymerization along the Z-axis. Once channels were successfully achieved, attempts were made to create a formulation with a lower dye concentration to assess if the good control of polymerization along the Z-axis could still be maintained. The devices obtained showed that in the case of the formulation with a low dye concentration, despite good definition, open channels could not be achieved.

Component	Name	%wt*
Monomer	TEGORad 2800	
Photoinitiator	BAPO in Omnirad (1:4 solution)	0.8
Dye	Methyl Red in MMA (1:7.5 solution)	0.075

* percentage by weight to resin

Component	Name	%wt*
Monomer	TEGORad 2800	
Photoinitiator	BAPO in Omnirad (1:4 solution)	0.8
Dye	MethylRed in MMA (1:50 solution)	0.85

* percentage by weight to resin

Table 4.6 TEGORad-based formulation with a lower concentration of Methyl Red (above) and with a higher concentration of Methyl Red (below)

Images of the devices obtained with both formulations are shown.

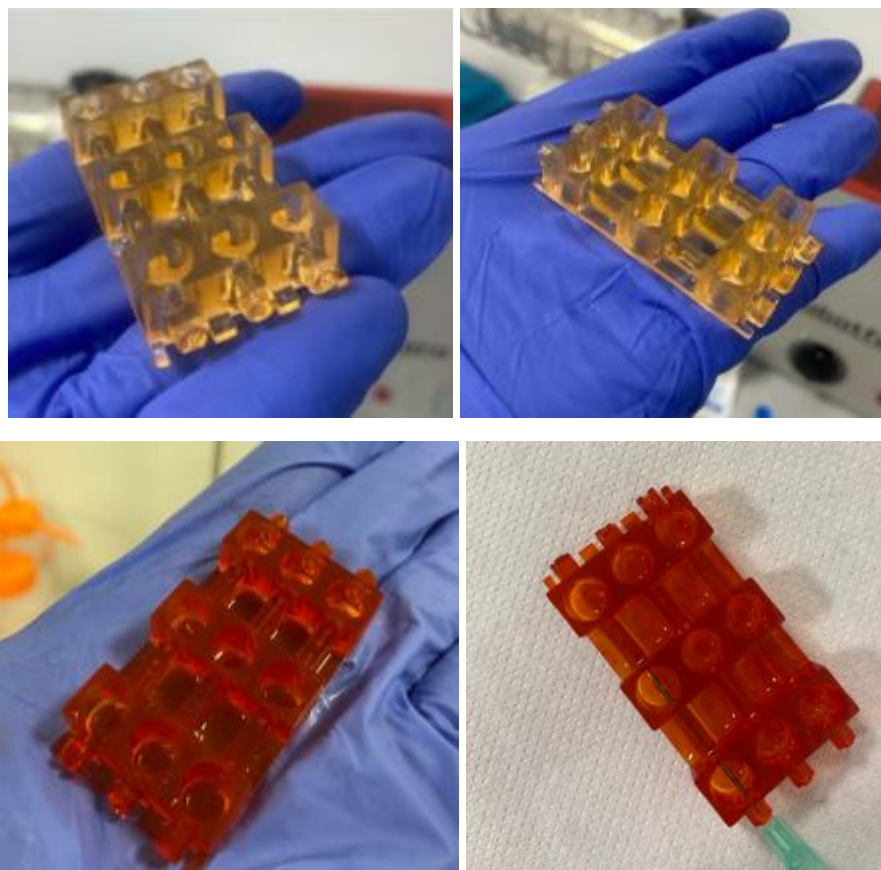


Figure 4.6 Smart plate obtained with a low concentration of Methyl Red (above) and with a high concentration of Methyl Red (below)

Although the last formulation led to the printing of a device with open channel, some studies regarding methyl red interaction with cells have suggested that its cytocompatibility varies depending on the type of cells and experimental conditions. In fact, although it can be used for vital staining under specific pH conditions, its cytocompatibility was not optimal in a study conducted on mixed bovine bone. Specifically, it was observed that Balb-c 3T3 cells underwent cell death when they came into contact with this dye. [50], [51]

Therefore, it was necessary to change the dye again. In choosing the new dye, a comparison was made among the dyes used, noting that greater control along the Z-axis was provided by the orange dye. This led to the selection of Disperse Red 1 methacrylate (DR1MA) as the dye. While the chromophore (azobenzene) is the

same for MR and DR1MA, the latter directly react with the polymeric matrix by radical co-polymerization of methacrylic moiety. This does not allow dye migration in contact with fluids, eliminating potential cytotoxic effects.

For Disperse Red 1 methacrylate, several formulations were developed, starting from higher concentrations of dye in solution and gradually reducing the amount, aiming to achieve open channels with a lower dye concentration. The tables below represent the tested formulations.

a)

Component	Name	%wt*
Monomer	TEGORad 2800	
Photoinitiator	BAPO in Omnirad (1:4 solution)	0.8
Dye	DR1-MA in MMA (1:20 solution)	0.85

* percentage by weight to resin

b)

Component	Name	%wt*
Monomer	TEGORad 2800	
Photoinitiator	BAPO in Omnirad (1:4 solution)	0.8
Dye	DR1-MA in MMA (1:30 solution)	0.85

* percentage by weight to resin

c)

Component	Name	%wt*
Monomer	TEGORad 2800	
Photoinitiator	BAPO in Omnirad (1:4 solution)	0.8
Dye	DR1-MA in MMA (1:40 solution)	0.85

* percentage by weight to resin

d)

Component	Name	%wt*
Monomer	TEGORad 2800	
Photoinitiator	BAPO in Omnirad (1:4 solution)	0.8
Dye	DR1-MA in MMA (1:50 solution)	0.85

* percentage by weight to resin

Table 4.7 TEGORad-based formulations (a) and (c) with higher concentrations of Disperse Red 1 methacrylate and (c) and (d) with lower concentrations of Disperse Red 1 methacrylate

Printing with higher concentrations of dye (formulations a and b) allowed for well-defined plates with unobstructed channels. Formulation d), which had a lower dye concentration, resulted in a well-defined plate, but the channels were partially obstructed. Therefore, an attempt was made to test an intermediate formulation, c), which achieved both good structural definition and free-flowing channels capable of allowing flow.

Figure 4.7 shows the concentration chosen for Disperse Red 1 methacrylate, while pictures 4.8 show the devices obtained from the printing process with formulation (c) given in Table 4.7.

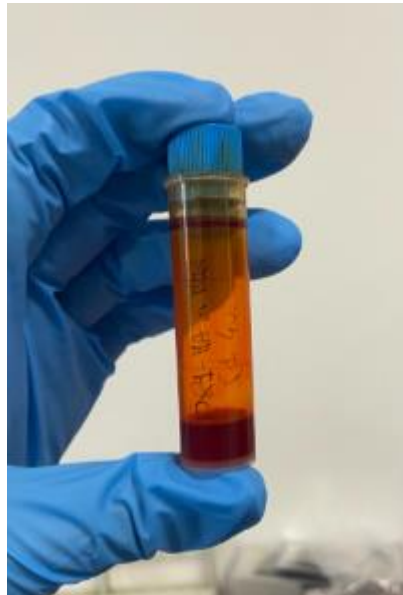
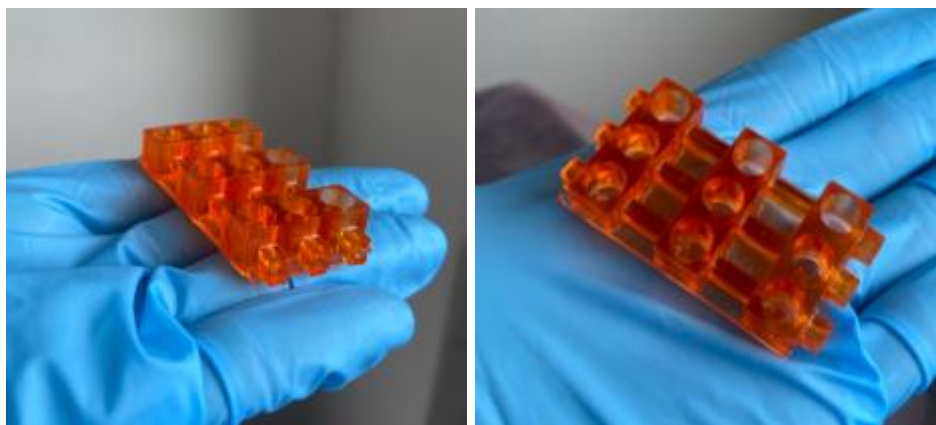


Figure 4.7 1:40 solution of Disperse Red 1 methacrylate in MMA



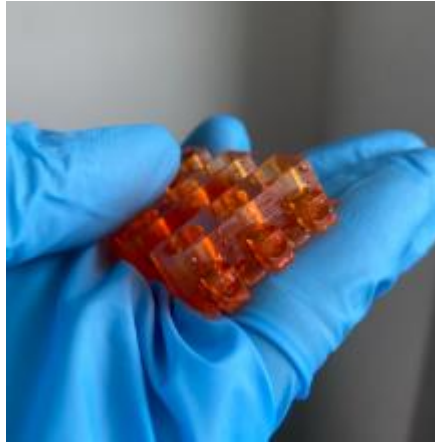


Figure 4.8 Smart plate with final formulation (Disperse Red 1 methacrylate)

The use of all dyes required their solubilization within methyl methacrylate (MMA).

4.3 PRINTING PARAMETERS OPTIMIZATION

In addition to defining appropriate formulations, it was necessary to establish correct printing parameters. The presence of different structures within the same device necessitated the definition of various printing ranges. For each defined range, considering the number of layers and the type of structure to be achieved, different parameters were selected. These parameters are defined and sent to the printer using specialized software, Asiga Composer. This software allows for the definition of all parameters; specifically, in this thesis work, the focus was primarily on defining the ranges and selecting exposure times. To create the smart plate, polymerization of 183 layers was necessary, divided as follows: the first 28 layers were in PEGDA, while the remaining layers were in TEGORad. The layers are grouped into ranges so that each range has its own parameters and enables the printing of specific geometries.

In this thesis work, 5 different ranges were defined: Burn-In and Range 1 for the PEGDA-based formulation, and Ranges 2 to 4 for printing with the TEGORad-based formulation. Although the various ranges represent different structures, there were some common parameters:

- Single layer thickness of 50 μm ;
- Minimum printing temperature set at 30°C;
- Maximum printing temperature set at 36°C.

Parameter setting was done differently for the two formulations. For the PEGDA-based formulation, since it is a widely used material in printing processes, we started from known parameters, which were then optimized through printing trials. For the TEGORad-based formulation, it was necessary, however, to take advantage of the printer's material test function. This type of test involves placing the resin in the tray, and then a spot is projected with varying exposure times. Once the projection is finished, the uncured resin is collected, and the cured layer is rinsed in isopropanol and measured using a caliper. The results of those test are reported in a graph showing the activation energy (mJ/cm^2) on the x-axis and the thickness on the y-axis (mm). A logarithmic trend line is reported for each formulation, also reporting the equation of the trend line in the form $y=mx+q$, where y represents the thickness and x represents the activation energy.

Material tests were carried out for all the formulations mentioned in Section 4.2.2. the results obtained are shown in the figure here:

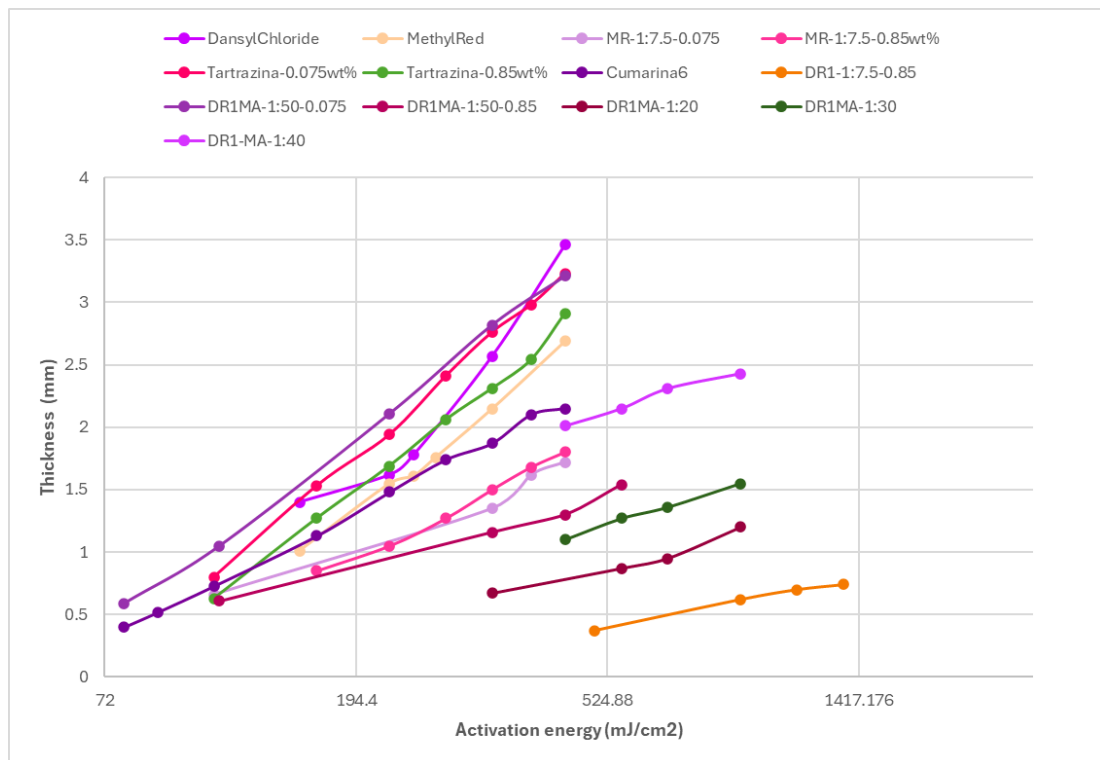


Figure 4.9 Material test

Observing the data, it appears evident that DR1MA allowed for the lowest irradiation times with the best resolution.

After conducting these tests, printing trials were carried out to further optimize exposure times. This allowed for the definition of parameters for ranges 2 to 4, successfully achieving all desired geometries.

Figure 4.10 shows the different optimized printing parameters, as well as the exposure times obtained through the previously analyzed tests.

Name	Burn-In	1	2	3	4	Units
Print Range From	0.000	0.100	1.400	5.000	7.600	mm
Print Range To	0.100	1.400	5.000	7.600	9.150	mm
Slice Thickness	0.050	0.050	0.050	0.050	0.050	mm
Heater Temperature	36.0	36.0	36.0	36.0	36.0	°C
Minimum Temperature	30.0	30.0	30.0	30.0	30.0	°C
Heater Enable	1	1	1	1	1	
Light Intensity	22.19	22.19	22.19	22.19	22.19	mW/cm ²
Light Intensity Control	1	1	1	1	1	
Exposure Time	3.000	3.000	12.500	14.000	15.500	s
Wait Time (After Exposure)	2.000	0.100	0.100	0.100	0.100	s
Wait Time (After Separation)	3.000	0.200	0.200	0.200	0.200	s
Wait Time (After Approach)	0.000	0.000	0.000	0.000	0.000	s

Figure 4.10 Optimized printing parameters

4.4 WASHING PROTOCOL

After obtaining the printed object, it was necessary to wash the obtained plate. Once the printing process was completed, it can happen that there are components in the formulation that did not react completely. These unreacted components may no longer be cytocompatible, even if all components of the initial formulation were cytocompatible. Therefore, a washing protocol was defined. Initially, a protocol defined in a previously conducted work was used. This protocol involved the following steps:

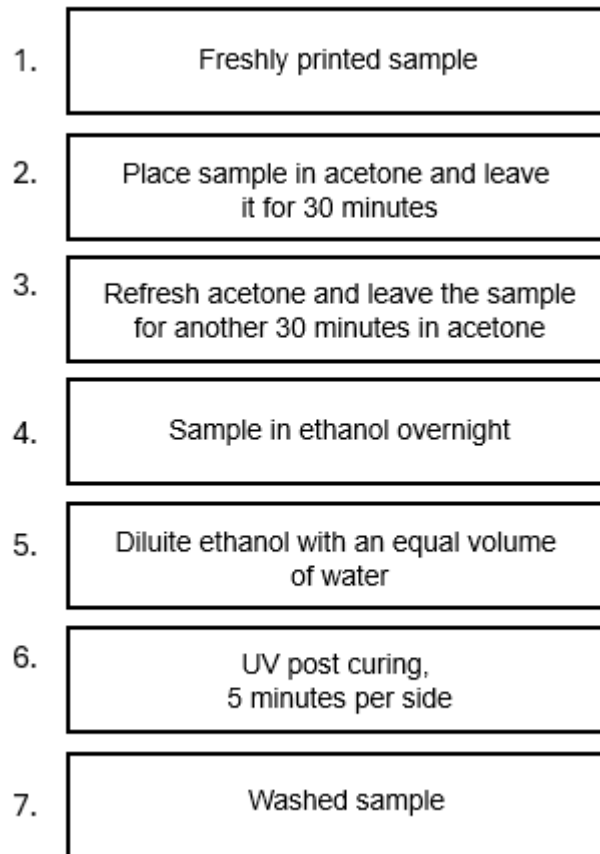


Figure 4.11 Initial washing protocol

Once this protocol was applied to the printed device, several issues emerged, such as swelling of the structure, warping of the base of the structure, and breaking of the well bases. To attempt to solve these issues, acetone was replaced with a less aggressive solvent, ethanol. After making this substitution, the protocol was tested using ethanol, comparing the structures washed in acetone with those washed in ethanol. The figures shown here demonstrate that replacing ethanol has allowed overcoming the issue of sample swelling (Figure 4.12) and the warping of the device base (Figure 4.13). However, as Figure 4.14 illustrates, simply replacing acetone with ethanol did not resolve the problem of well base breakage.

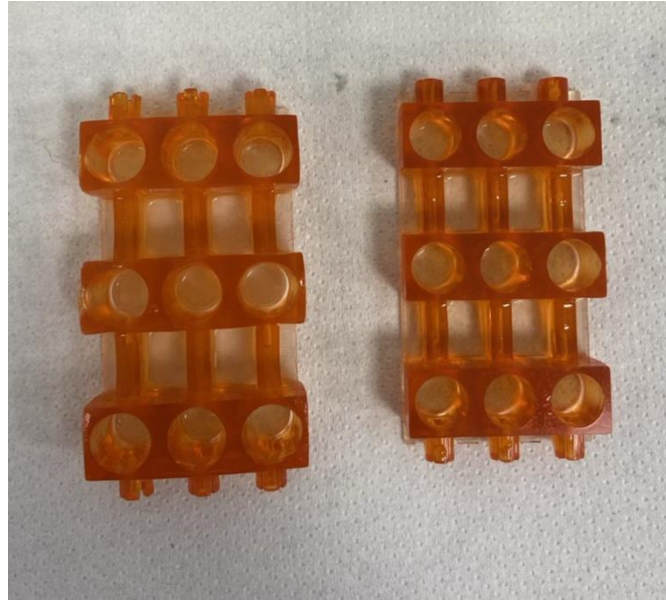


Figure 4.12 Swelling sample placed in acetone (left) and sample placed in ethanol (right)

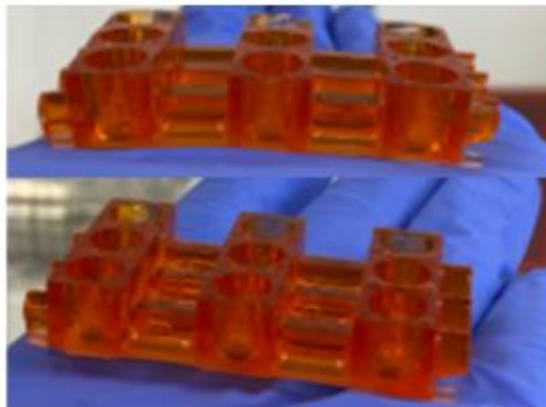


Figure 4.13 Embedding sample placed in acetone (left) and sample placed in ethanol (right)

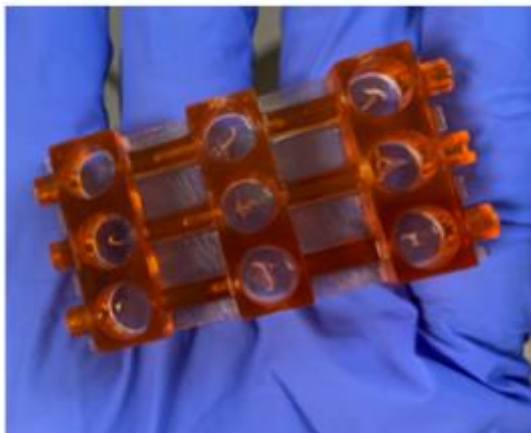


Figure 4.14 Base-well breakage

To overcome the issue of well base breakage, in addition to replacing acetone with ethanol, a UV post-curing phase of 5 minutes per side was considered before immersing the sample in the solvent for various time steps. Before finalizing the new protocol, spectra of the solutions containing the plates at different time steps (first 30 minutes, second 30 minutes, and overnight) were studied, comparing solutions containing acetone versus those containing ethanol. The results shown in the graph in Figure 4.15 indicate no significant differences, leading to the adoption of the new protocol.

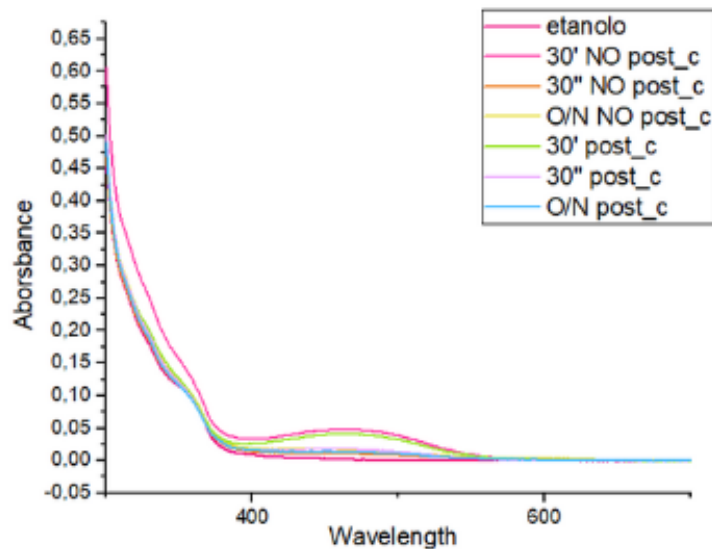


Figure 4.15 Comparison of absorbance values for solutions containing post-cured and uncured samples.

The results made it possible to define the new protocol, which includes the following steps:

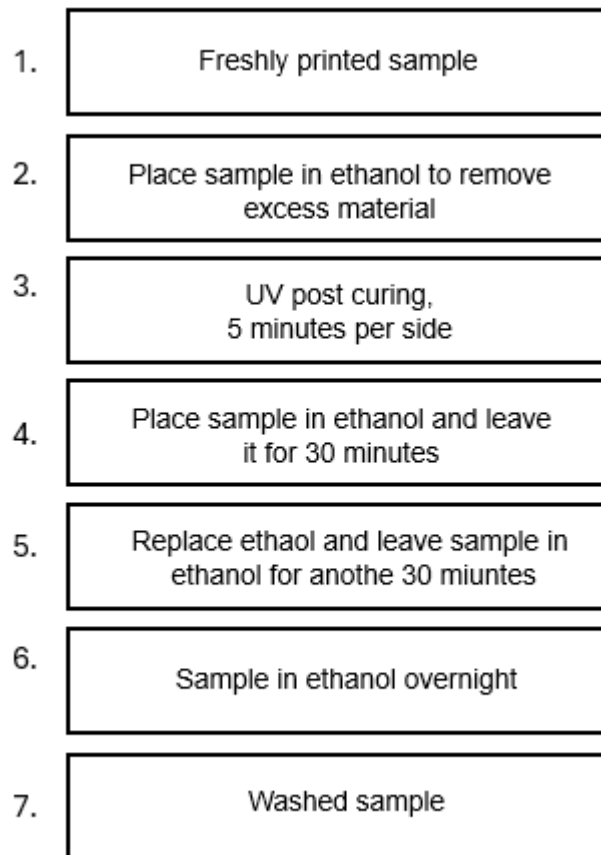


Figure 4.16 Optimized washing protocol

Once the new protocol was defined, it was tested on the printed device. Adding the post-curing phase immediately after printing helped overcome the issue of well base breakage, as shown in Figure 4.17.

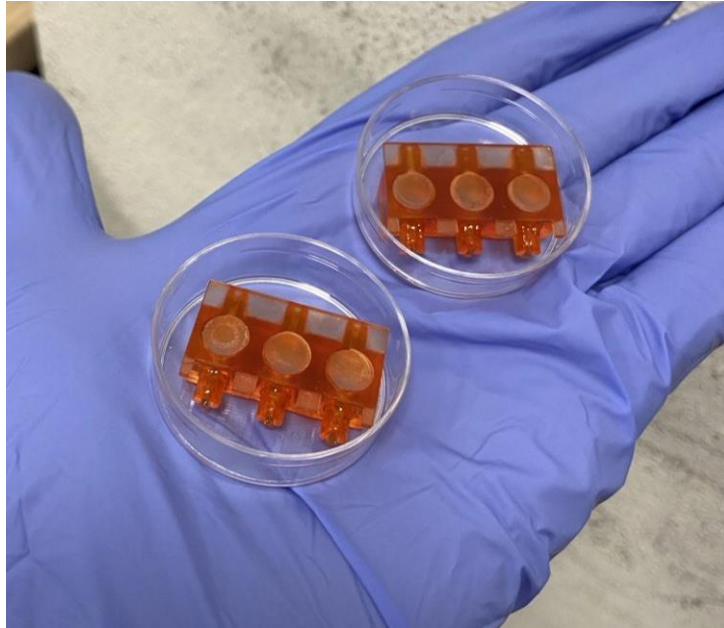


Figure 4.17 Absence of well breakage in post-cured samples

4.5 MICROFLUIDIC SIMULATIONS AND TESTS

After printing and washing the device, the fluidics of the obtained smart plate were studied. Before conducting direct tests on the plate, simulations were performed using two different software programs, Solidworks and Comsol. The first software was used to fill the wells with fluid. Once the wells were filled, the model was loaded into Comsol, which allowed for various flow simulations. Each simulation provided maximum velocity and pressure values occurring inside the device. For each flow, it was possible to obtain images of pressure distribution and flow lines throughout the device, as well as flow lines at the base of the wells, which are crucial for the analysis of cells that will be placed at the bottom of the wells. The following flows were analyzed, along with their respective maximum velocity and pressure values, and graphs depicting the pressure distribution and flow lines in the device and at the base of the wells:

- $f_1 = 50 \mu\text{l}/\text{min}$ ($8.33\text{E}-10 \text{ m}^3/\text{s}$)

Maximum flow rate (m/s)	Maximum Pressure (Pa)
0.004	0.931

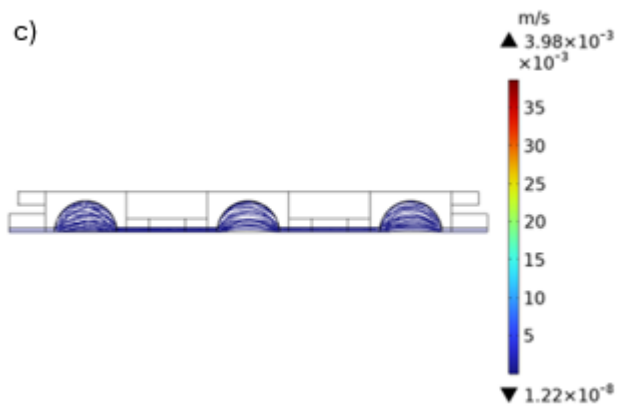
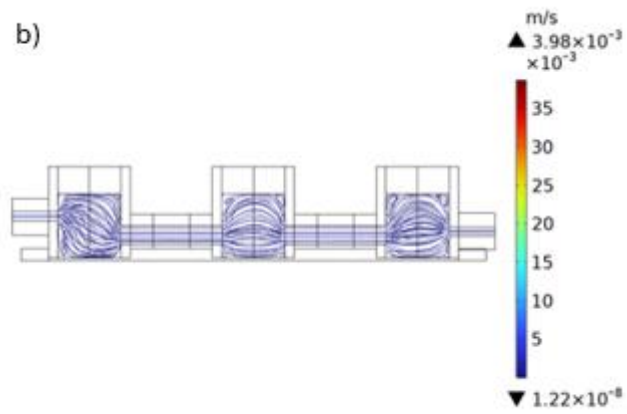
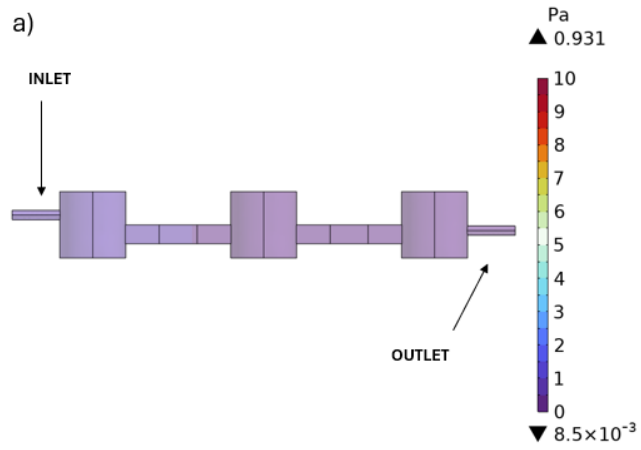
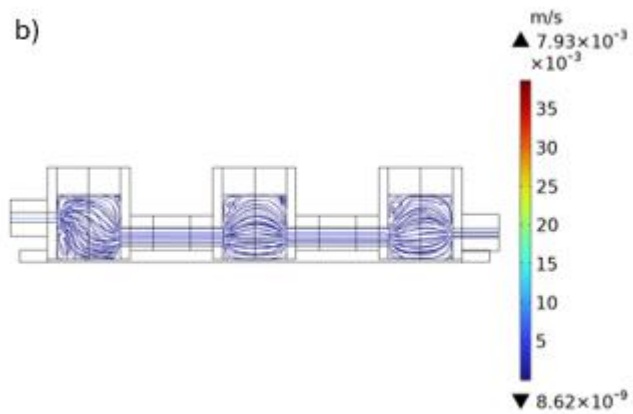
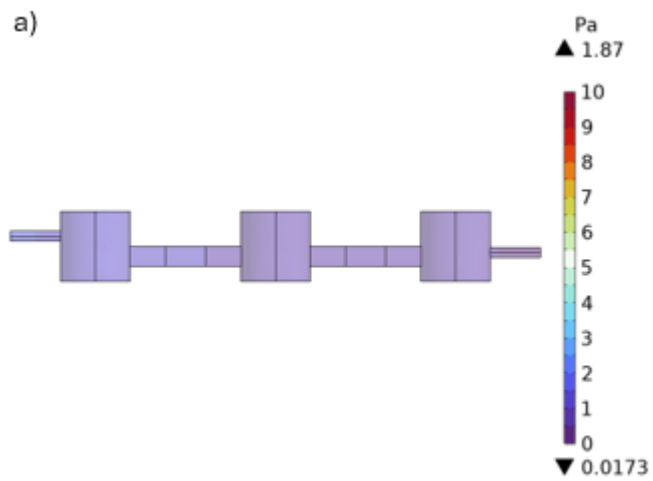


Figure 4.18 Trends of (a) pressure (b) stream lines in the device and (c) stream lines at the base of the wells for $f_1=50 \mu\text{l}/\text{min}$

- $f_2= 100 \mu\text{l}/\text{min}$ ($1.67\text{E-}9 \text{ m}^3/\text{s}$)

Maximum flow rate (m/s)	Maximum Pressure (Pa)
0.009	1.870



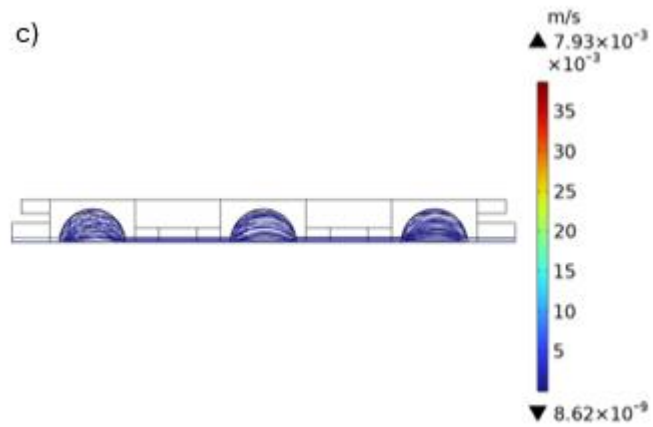
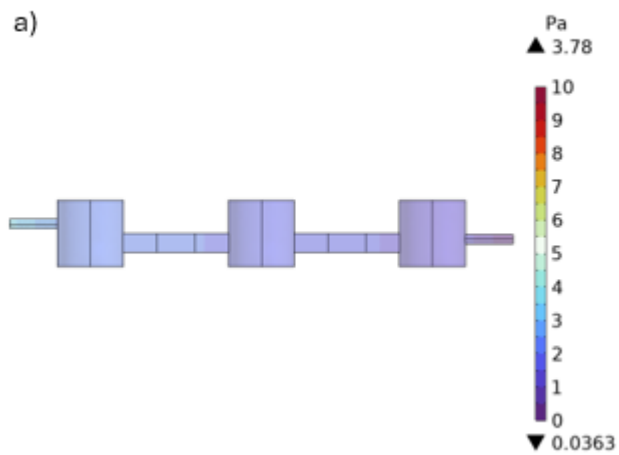


Figure 4.19 Trends of (a) pressure (b) stream lines in the device and (c) stream lines at the base of the wells for $f_2=100 \mu\text{l}/\text{min}$

- $f_3= 200 \mu\text{l}/\text{min}$ ($3.33\text{E-}9 \text{ m}^3/\text{s}$)

Maximum flow rate (m/s)	Maximum Pressure (Pa)
0.018	3.784



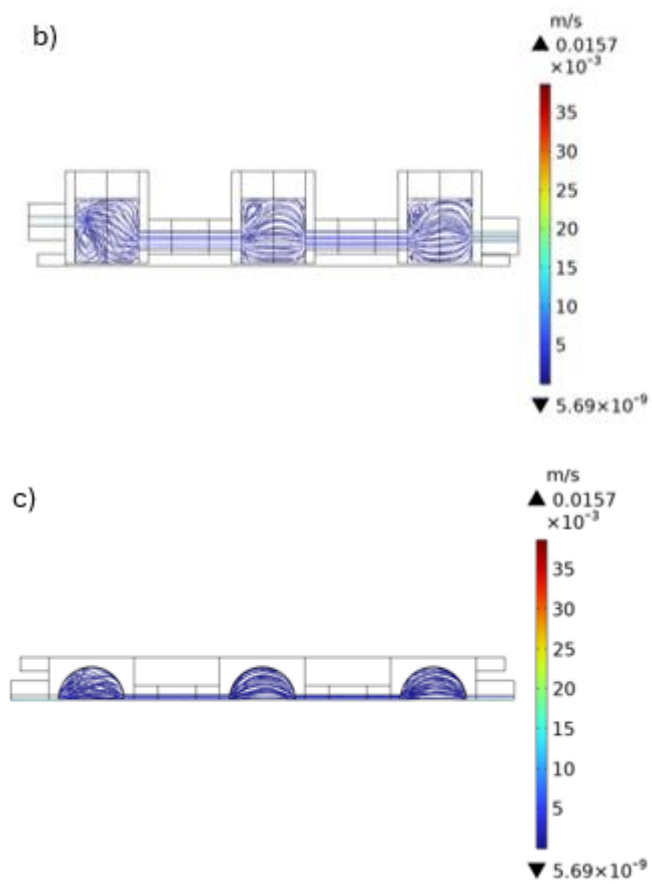


Figure 4.20 Trends of (a) pressure (b) stream lines in the device and (c) stream lines at the base of the wells for $f_3=200 \mu\text{l}/\text{min}$

- $f_4 = 300 \mu\text{l}/\text{min}$ ($5.00\text{E-}9 \text{ m}^3/\text{s}$)

Maximum flow rate (m/s)	Maximum Pressure (Pa)
0.026	5.765

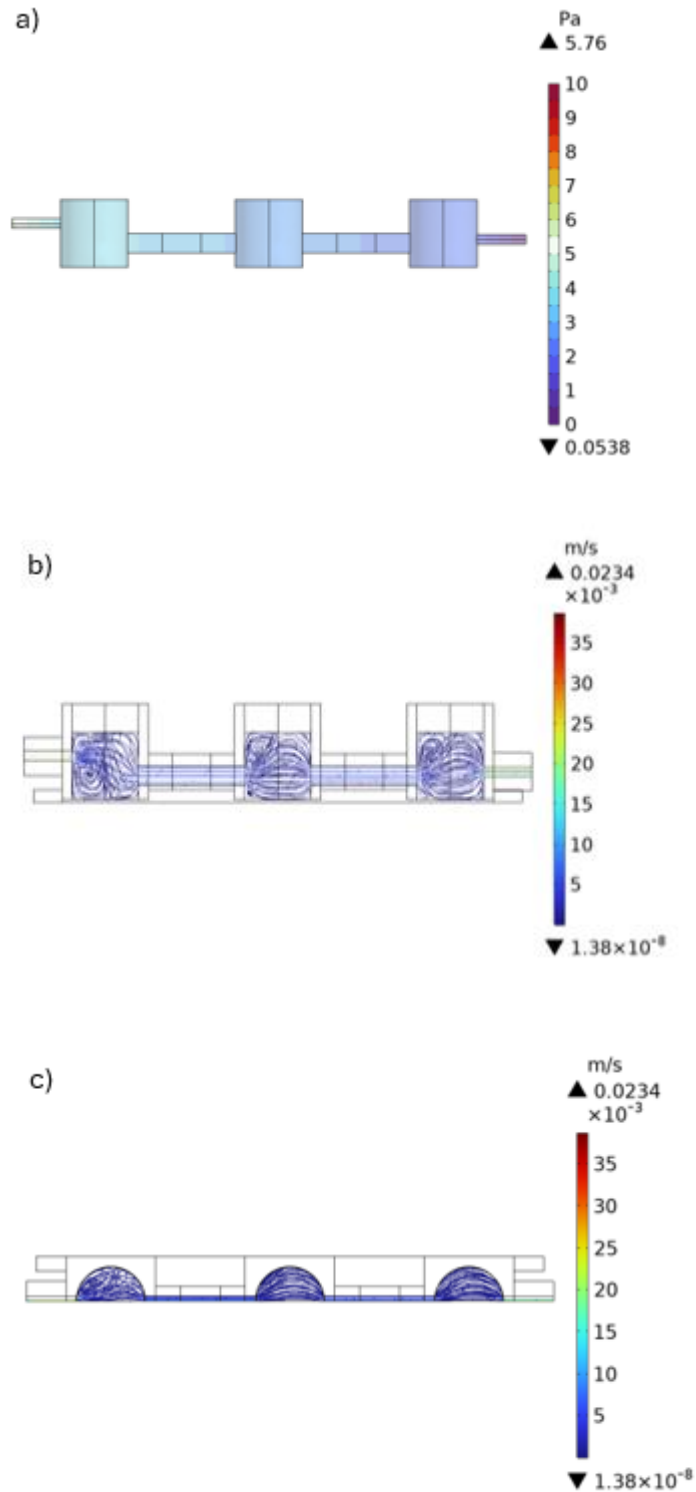
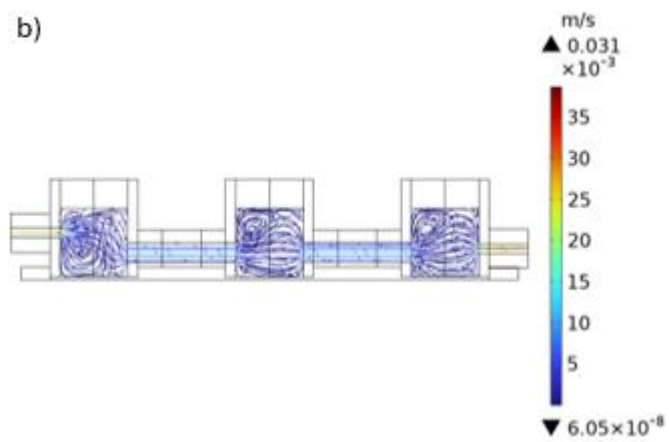
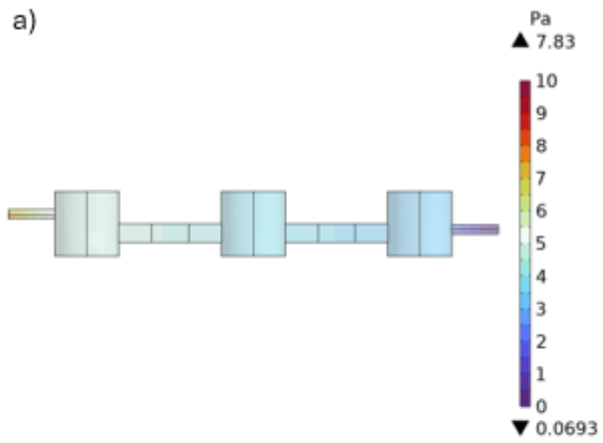


Figure 4.21 Trends of (a) pressure (b) stream lines in the device and (c) stream lines at the base of the wells for $f_4 = 300 \mu\text{l}/\text{min}$

- $f_5 = 400 \mu\text{l}/\text{min}$ ($6.67 \times 10^{-9} \text{ m}^3/\text{s}$)

Maximum flow rate (m/s)	Maximum Pressure (Pa)
0.035	7.829



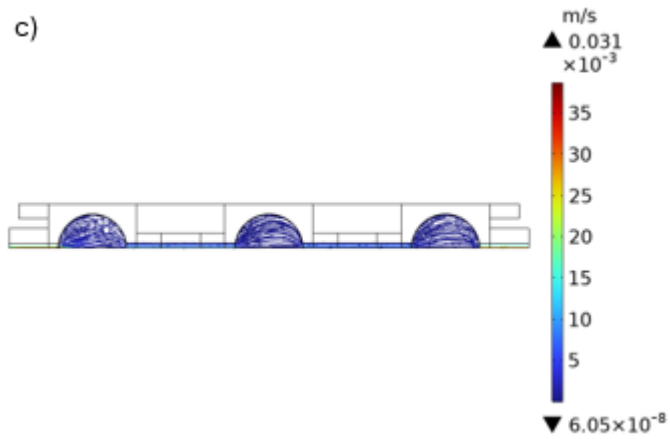
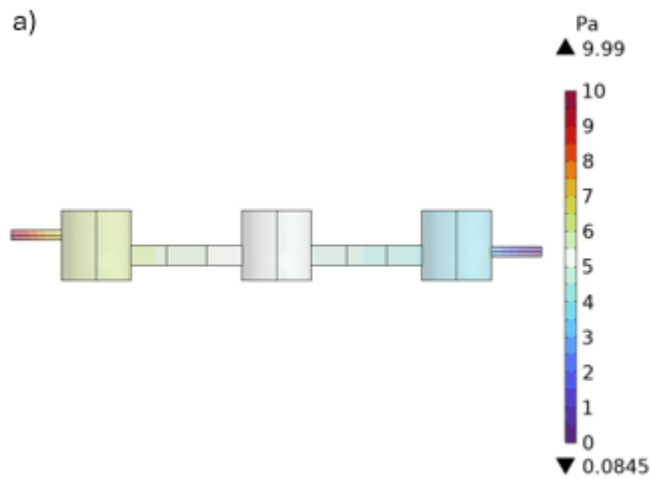


Figure 4.22 Trends of (a) pressure (b) stream lines in the device and (c) stream lines at the base of the wells for $f_5=400 \mu\text{l}/\text{min}$

- $f_6= 500 \mu\text{l}/\text{min}$ ($8.33\text{E-}9 \text{ m}^3/\text{s}$)

Maximum flow rate (m/s)	Maximum Pressure (Pa)
0.043	9.986



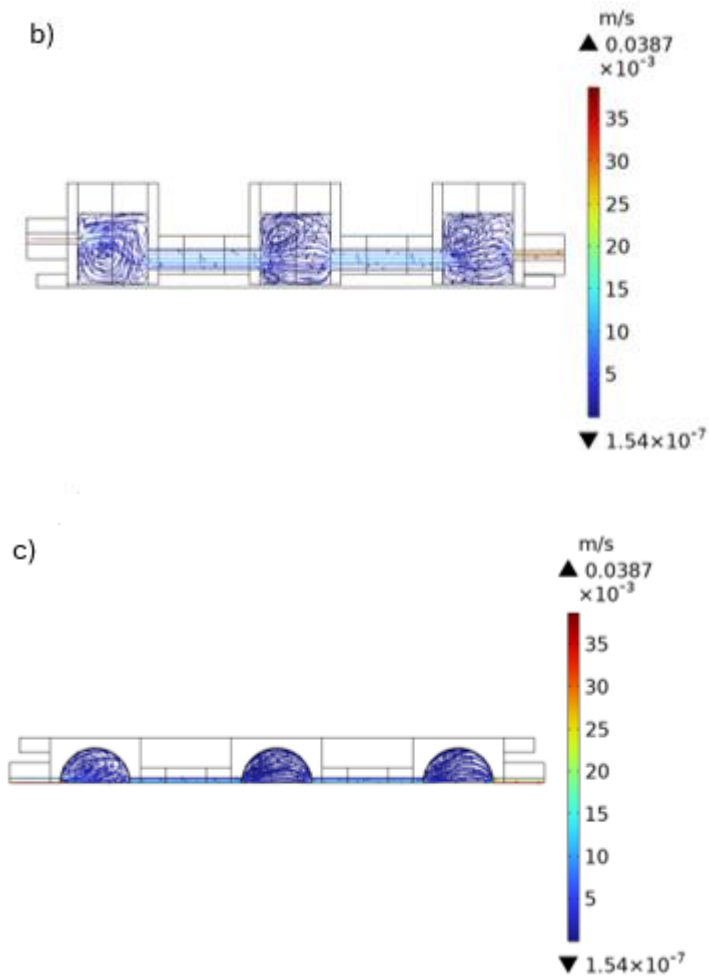


Figure 4.23 Trends of (a) pressure (b) stream lines in the device and (c) stream lines at the base of the wells for $f_5=400 \mu\text{l}/\text{min}$

The simulations not only allowed for the calculation of maximum pressure and velocity values occurring within the device but also enabled the observation of the pressure distribution and streamlines throughout the device, as well as the streamlines at the base of the wells. This latter aspect is particularly interesting considering the intended applications of the developed device, as the cells will be placed at the base of the wells. However, despite the obtained distribution, due to the failure of the cell cultured in the plate to survive, as explained in paragraph 4.6.4, it was not possible to evaluate the similarity between the values obtained in the simulations and those that could be obtained in vivo, and to determine whether, within these ranges, the cells are able to survive.

Starting from the data obtained in the simulation, direct plate tests were performed. In order to carry out these tests, a UV lamp was used so that the tubes could be connected as shown in Figure 4.24, and a 1:50 solution of ddH₂O and Disperse Blue 1 was prepared so that we could observe what is happening inside the plate. The pump chosen to carry out the tests on the smart plate is a 2-head peristaltic pump, the LiveFlow (IVTech), which allows working with flow rates that fall in the range of 50 to 500 $\mu\text{l}/\text{min}$. The experiments were conducted with two different flow rates:

- $f_1 = 100 \mu\text{l}/\text{min}$;
- $f_2 = 250 \mu\text{l}/\text{min}$.

The first test lasted 10 days, while the second test was run for the entire weekend (48 hours). The experiments conducted underscored the feasibility of making processes such as the change of the culture medium needed in cell cultures automated. In contrast to the simulations performed in which the wells were found to be occupied by the same amount of solution from the start, the direct plate experiments showed an initial phase in which the wells were characterized by different fluid heights, heights that, however, after about two hours all became equal, bringing the device into a steady state. The longest experiment showed that the steady state of the device was maintained even after 10 days: at the tenth day, in fact, the wells all had the same of fluid level and the same solution coloration (complete diffusion of the dye).

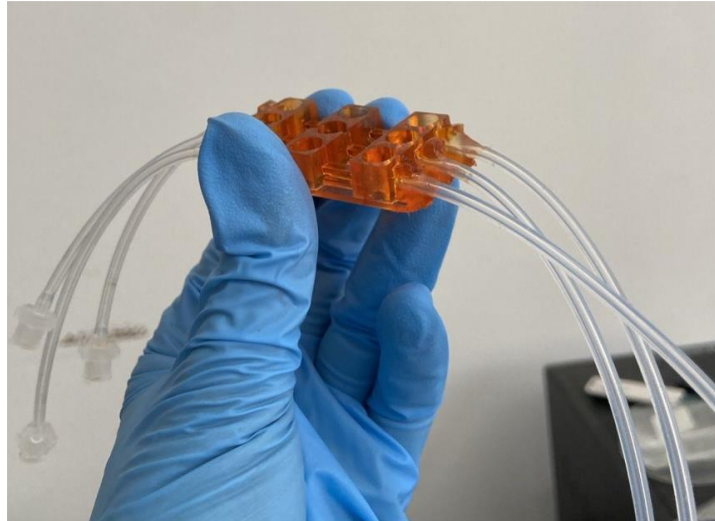


Figure 4.24 Cable connection by using UV lamp



Figure 4.25 Set-up for experimental test on smart plate



Figure 4.26 Plate at day 10 of flow; maintaining steady state

4.6 BIOLOGICAL CHARACTERIZATIONS AND TESTS

Once the device had been obtained and, after testing the operation of the fluidics, it was necessary to conduct characterizations of the plate to test its use in bio. In addition to the characterization of the plate, this chapter will also discuss the results obtained from some bio tests conducted on the smart plate.

4.6.1 FLUORESCENCE

The first characterization was carried out through the Synergy HTX plate reader. Specifically, 3 different pairs of excitation/emission wavelengths were analyzed to study the signal emitted within these ranges of the obtained smart plate and compare it with the signal emitted in the same ranges of a normal polystyrene laboratory plate. The ranges studied are:

- 360/460 nm;
- 485/528 nm;
- 539/590 nm.

For each of these analyzed intervals, individual values were obtained, as shown in Figure 4.27. Specifically, there are 3 values for each well: the first indicates the value of the emitted fluorescence signal in the first interval studied, the second indicates the value of the emitted fluorescence signal in the second interval and the third in the third interval. A comparison was then made between the normal polystyrene plate (Figure 4.27 above) and the smart plate (Figure 4.27 below) to determine whether the latter could be used in this instrument to read cell signals.

	1	2	3	4	5	6	7	8	9	10	11	12
A	5		9		14			6		10		13
	1		7		8			1		8		7
	2		8		9			1		9		7
B	13		7		12			13		7		12
	10		3		2			10		2		4
	10		3		3			9		2		4
C	15		11		8			17		11		8
	9		2		3			8		2		4
	9		2		5			7		1		6
F	14		16		9			16		14		7
	9		8		1			10		5		1
	3		4		10			0		7		7
G	10		9		16			10		10		15
	5		2		9			3		4		10
	7		8		1			10		3		4
H	9		8		15			9		9		14
	6		1		8			4		1		9
	3		4		10			1		8		8

	1	2	3	4	5	6	7	8	9	10	11	12
A	9		6		2			8		3		7
	0		6		7			1		7		8
	12		5		3			11		10		3
B	4		11		6			2		10		11
	7		2		5			7		1		5
	5		10		8			9		11		4
C	2		9		9			3		10		9
	9		3		3			10		5		1
	3		9		9			6		4		11
F	8		11		3			11		4		5
	1		5		9			4		9		2
	13		5		7			5		5		12
G	8		12		3			2		11		9
	10		2		5			9		8		0
	5		10		10			7		3		11
H	4		7		11			4		13		6
	9		3		4			4		3		9
	5		13		9			11		9		4

Figure 4.27 Signals emitted by the polystyrene plate (top) and the smart plate (bottom)

The results shown in Figure 4.27 show that the signals emitted by both plates are comparable to each other, thus suggesting the possibility of using the smart plate to read cell signals using the same plate reader (Synergy HTX plate reader) used with polystyrene plate.

4.6.2 CYTOTOXICITY

Since the goal of this thesis work is to create a device for cell cultures and drug testing, it was necessary to investigate the potential cytotoxicity of the material chosen for the smart plate. To test cytotoxicity, the conditioned media test was

performed, involving the insertion of the smart plate into the culture medium for an entire weekend. After the weekend, the medium was collected and used for cell culture. Subsequently, a cell viability assay, MTT, was performed. MTT is a yellow-colored salt that turns purple when taken up by cells, indicating the presence of metabolically active cells if the solution in the wells turns purple. In parallel, a cell culture was performed using the same culture medium that did not come into contact with the material. For cytotoxicity assessment, two different cell lines were analyzed:

- Human fibroblast (HFF1) provided by ATCC;
- Human keratinocytes (HaCaT) provide by Antibody Research Corporation;
- Endothelial cells (EC) kindly gifted by IRCCS Candiolo Institute.

Based on the cells used, different culture media were employed:

- For Hacat and HFF1 cells: DMEM GlutaMAX supplemented with 15% Fetal Bovine Serum, 1% penicillin-streptomycin, 1% L-glutamine, 1% sodium pyruvate;
- For EC cells: a 1:1 mixture of DMEM GlutaMAX (supplemented as previously described) and F12K supplemented with 10% Fra Bovine Serum, 1% penicillin-streptomycin, 0.01 mg/ml Heparin and brain extract supplement.

Using the Synergy HTX plate reader, measuring absorbance at specific wavelengths: 570 nm to read MTT and 650 nm to subtract the polystyrene signal of the plate. The signal from cells cultured in normal medium was used as a control. The same procedure was repeated on cells cultured for 72 hours in conditioned medium. Differences between groups were analyzed using two-way ANOVA.

The graph here shows the results regarding the HaCats obtained, which were analyzed using two-way ANOVA.

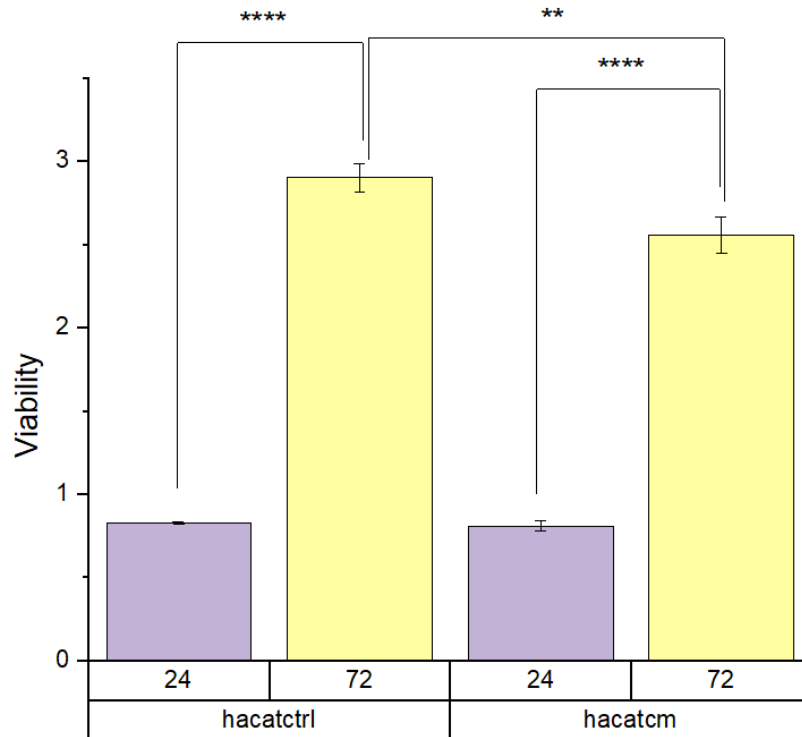


Figure 4.27 HaCaT viability comparison at 24h and 72h in culture medium and conditioned medium. Results analyzed with 2-way Anova.

Then the microscopically observed images of HaCaTs at 24 h and 72 h without (Figures 4.28) and with MTT (Figures 4.29) are shown.

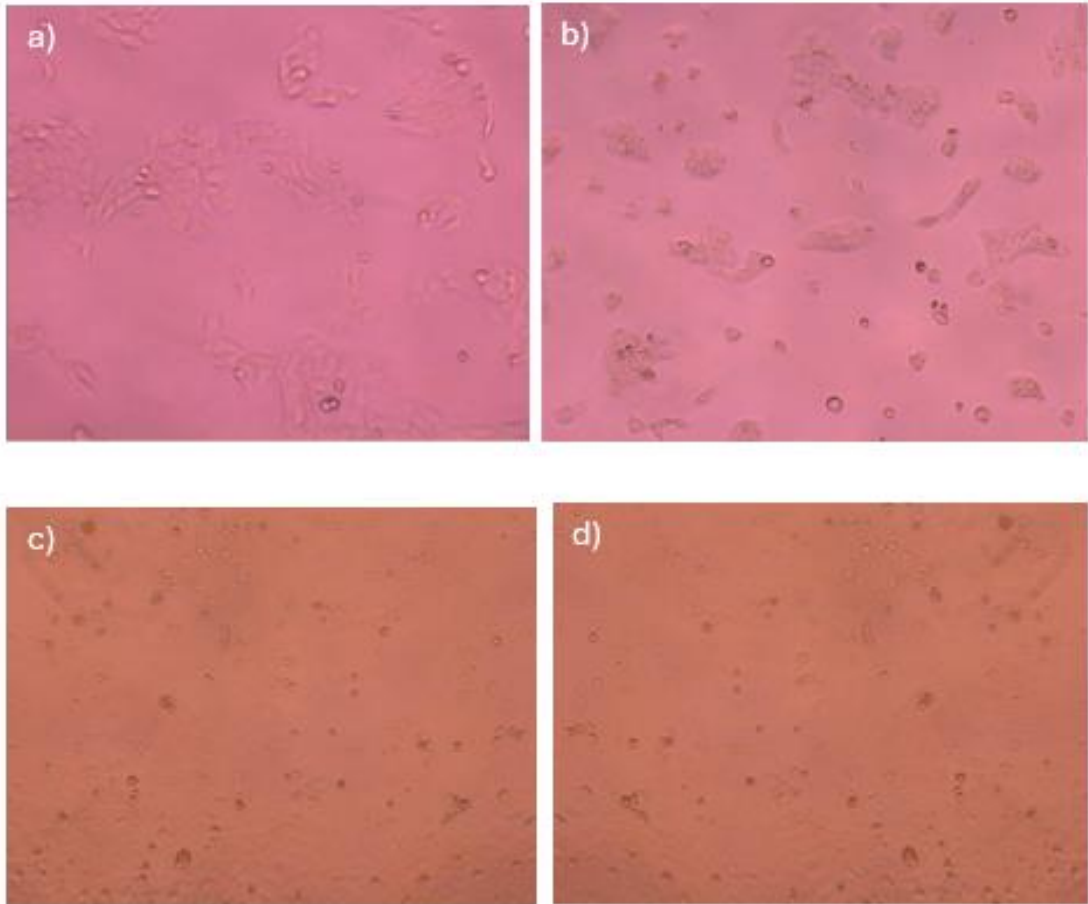


Figure 4.28 HaCaT without MTT (a) in the control medium and (b) in the conditioned medium at 24h (c) in the control medium and (d) in the conditioned medium at 72h

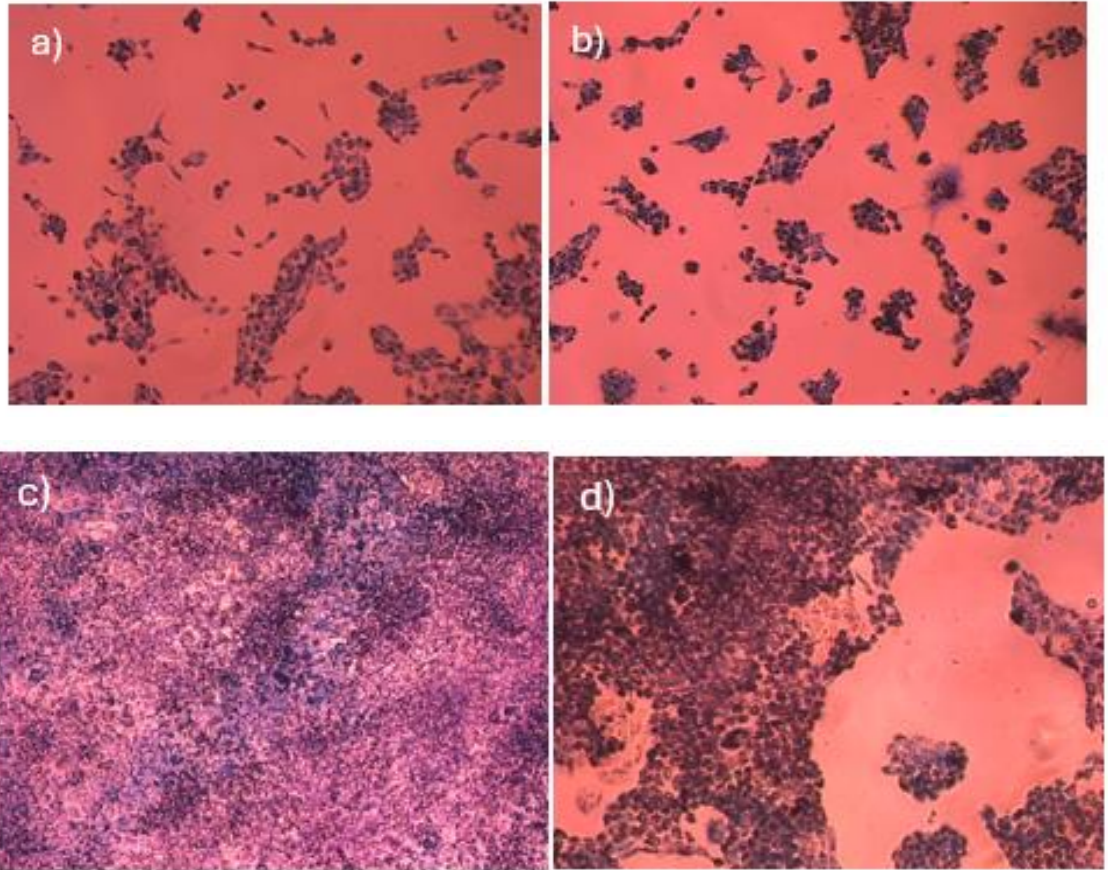


Figure 4.29 HaCaT with MTT (a) in the control medium and (b) in the conditioned medium at 24h (c) in the control medium and (d) in the conditioned medium at 72h

The graph here shows the results regarding HFF1 obtained, analyzed with two-way ANOVA.

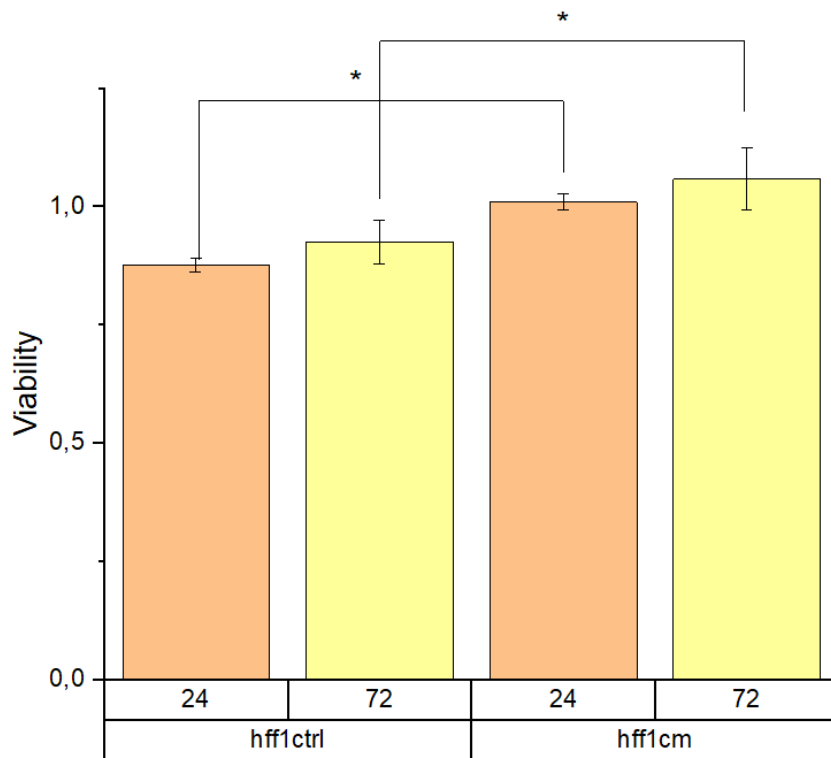


Figure 4.30 HFF1 viability comparison at 24h and 72h in culture medium and conditioned medium. Results analyzed with 2-way Anova.

Also in this case, the images observed under a microscope of HFF1 cells at 24 h and 72 h are then shown without (Figure 4.31) and with MTT (Figure 4.32).

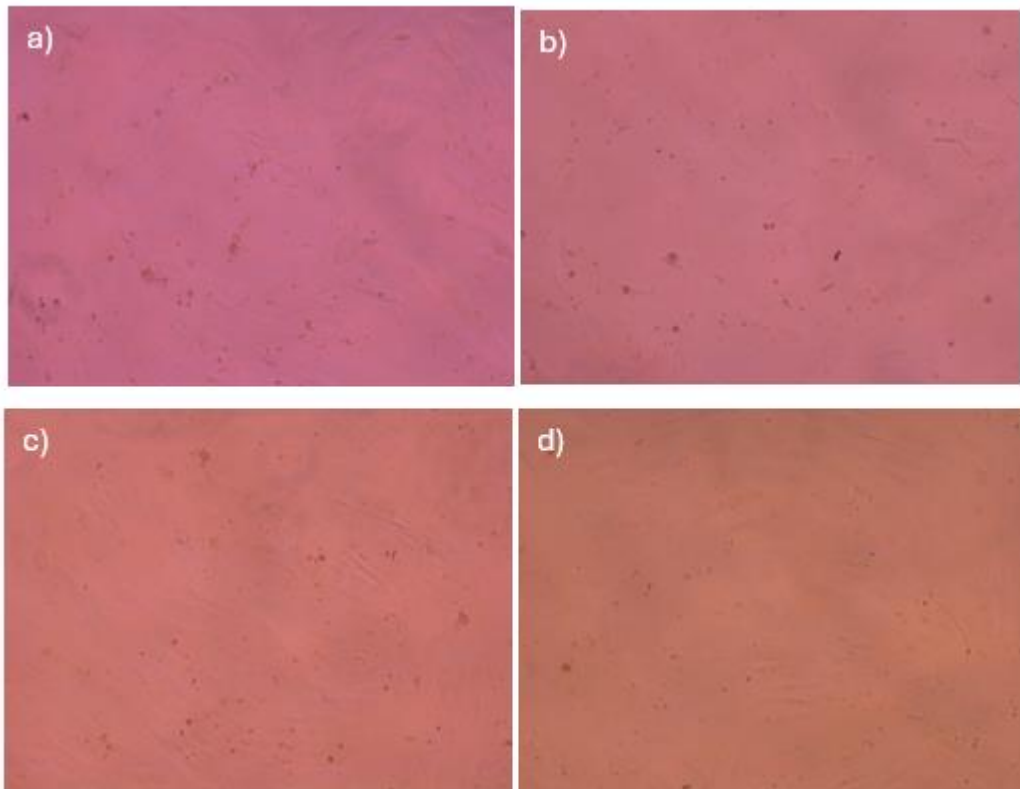


Figure 4.31 HFF1 without MTT (a) in the control medium and (b) in the conditioned medium at 24h (c) in the control medium and (d) in the conditioned medium at 72h

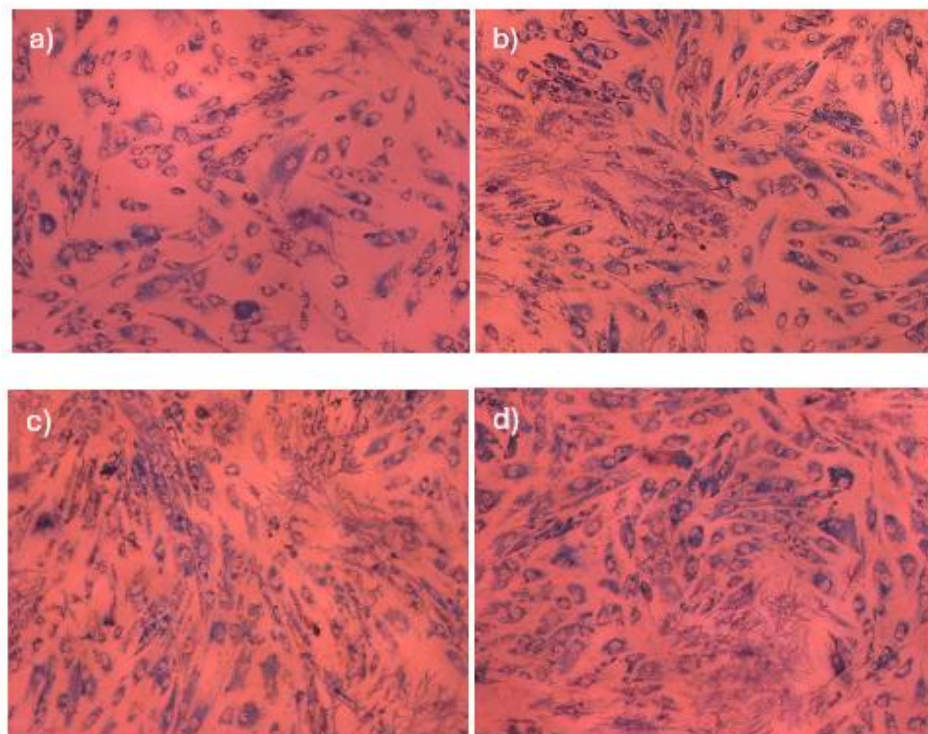


Figure 4.32 HFF1 with MTT (a) in the control medium and (b) in the conditioned medium at 24h (c) in the control medium and (d) in the conditioned medium at 72h

The last graph shows the results regarding EC obtained, analyzed with two-way ANOVA.

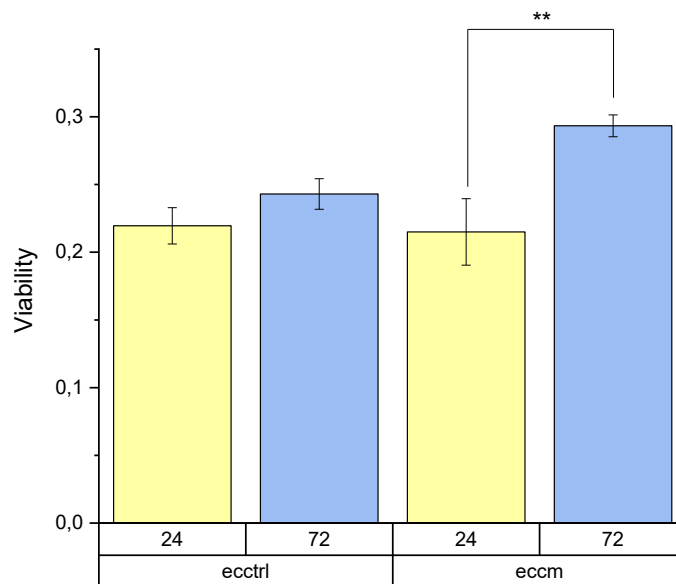


Figure 4.33 EC viability comparison at 24h and 72h in culture medium and conditioned medium. Results analyzed with 2-way Anova.

In this case, due to unavailability of the instrument it was not possible to microscopically observe images of EC cells at 24h and 72h with and without MTT.

For all three cell lines analyzed, the results show that the cells tend to proliferate between 24 and 72 hours in both culture medium and conditioned medium. These results allow us to conclude that the formulation chosen to manufacture the device is not cytotoxic, allowing us to proceed with experimentation to study the direct interaction of the cells with the device.

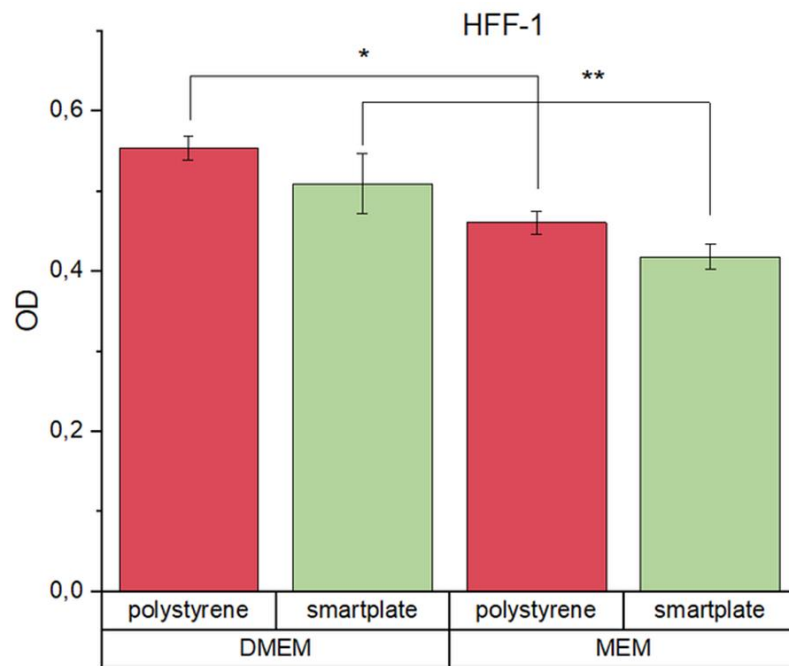
4.6.3 INTERACTION BETWEEN MATERIAL AND CELLULAR ASSAY

After conducting the conditioned medium tests on the two different cell lines, it was necessary to investigate a possible interaction between the MTT and the material chosen to make the device in order to demonstrate the veracity of the results obtained. HFF1s were seeded in two different types of culture medium:

- DMEM: high glucose culture medium;

- MEM: low-glucose culture medium.

Once the cell cultures were completed, the MTT cell viability assay was performed. The solution containing MTT was then sampled and initially read in the wells of the polystyrene plate, followed by the wells of the smart plate. Absorbances were analyzed using the Synergy HTX plate reader. To ensure result robustness, experiments were conducted in duplicate. Data analyses were performed using two-way ANOVA. The results are shown in the figure 4.34.



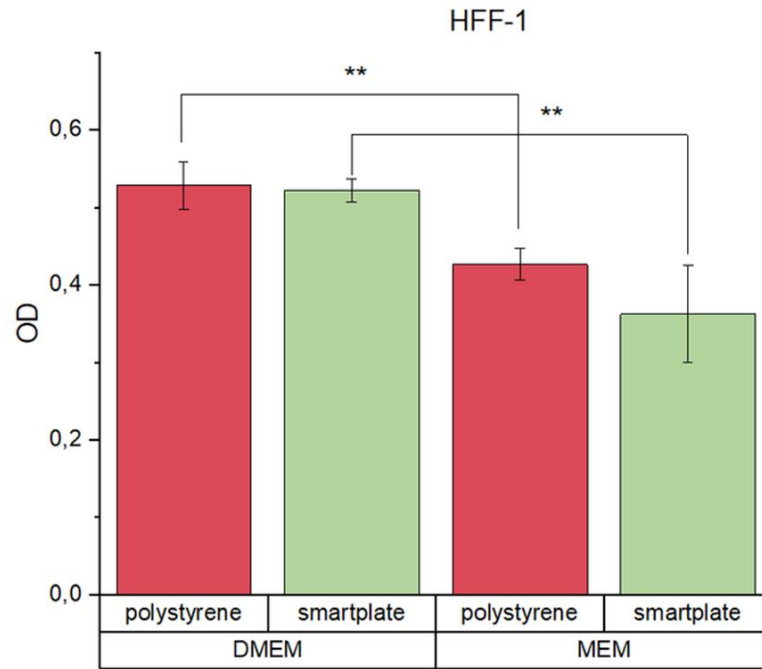


Figure 4.34 MTT reading in the polystyrene plate and smart plate. Analysis by 2-way Anova.

The results obtained show no significant difference in cell viability. The graphs also demonstrate that statistical differences between the two different culture media are maintained. This allow us to assert that the results obtained to assess the cytotoxicity of the material through the conditioned medium tests (paragraph 4.6.2) are not influenced by any potential interaction between the material used and the chosen cellular assay (MTT). These findings represent an initial indication of the potential compatibility of the chosen formulation with cells.

4.6.4 VITALITY AND CELL PROLIFERATION

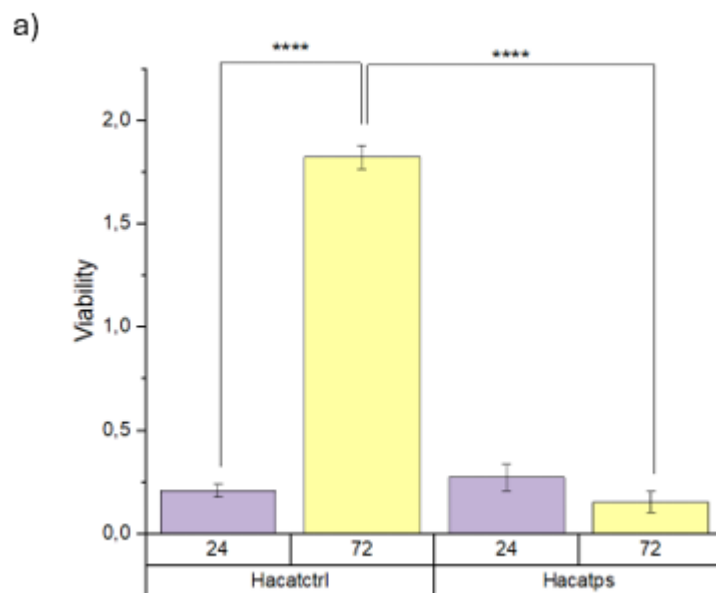
With the aim of testing cell viability and cell proliferation directly on the plate, gelatin coating was applied to facilitate cell cultivation on the smart plate. This coating enabled the exposure of RGD groups responsible for cell adhesion.

Three different cell types were analyzed:

- Human fibroblast (HFF1) provided by ATCC;
- Human keratinocytes (HaCaT) provide by Antibody Research Corporation;
- Endothelial cells (EC) kindly gifted by IRCCS Candiolo Institute.

The first two, HaCaT and HFF1, are cell lines, while ECs are primary cells. HaCaT and HFF1 cells were cultured in DMEM supplemented with 15% Fetal Bovine Serum, 1% penicillin-streptomycin, 1% L-glutamine, and 1% sodium pyruvate. ECs were cultured in F12K supplemented with 10% Fetal Bovine Serum, 1% penicillin-streptomycin, 0.01 mg/ml Heparin, and brain extract supplement. For all three cell types, analyses were conducted at different time points, 24 h and 72 h, involving cell cultures using the same cell types but on a standard laboratory multiwell polystyrene plate as a control.

Below are the results obtained for the study of cellular vitality for all three types of cells investigated.



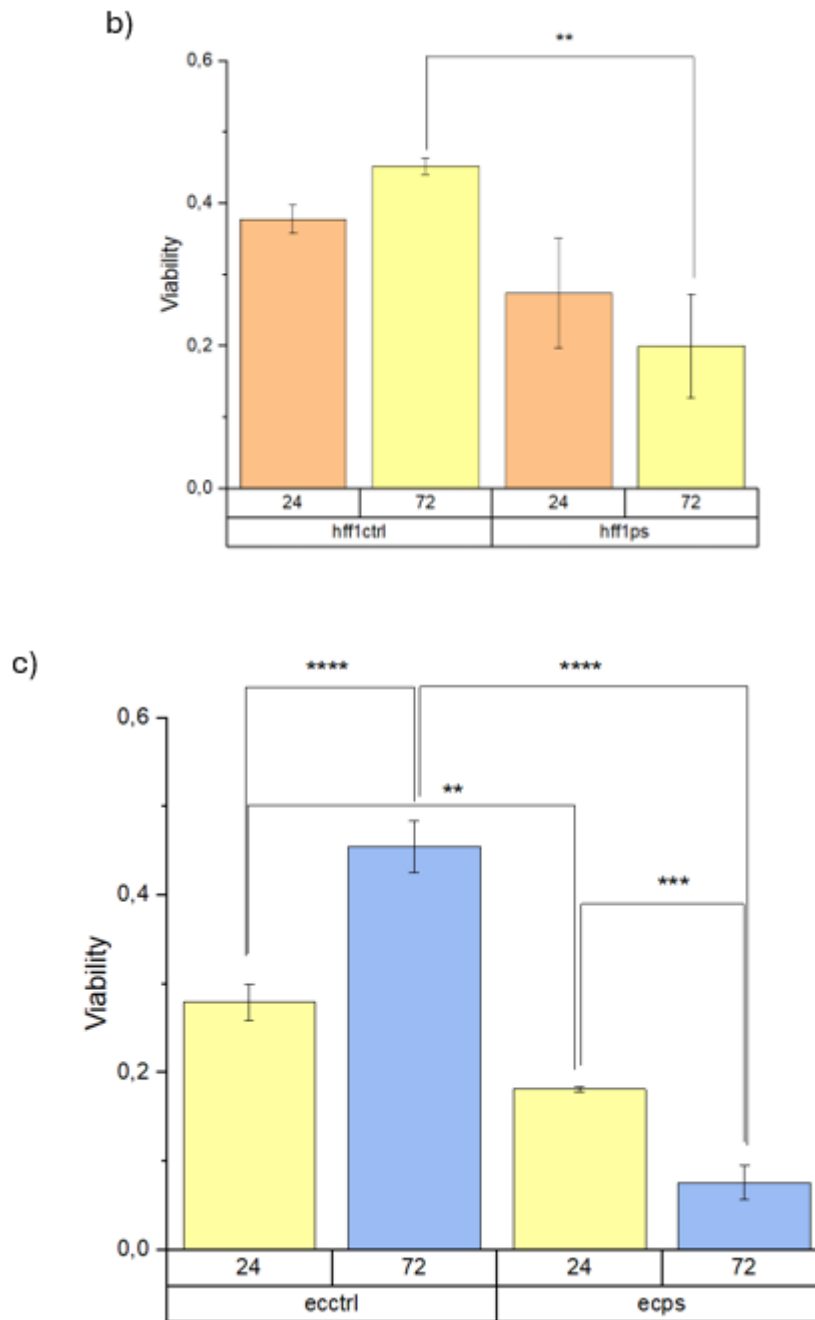


Figure 4.35 Viability of (a) HaCaT (b) HFF1 and (c) EC on polystyrene plate and smart plate. Analysis by 2-way Anova.

The above graphs obtained through two-way ANOVA show that, in the case of cells cultured on the polystyrene plate, they tend to proliferate between 24h and 72h. However, for cells cultured on the smart plate, there is a tendency towards cell death between 24h and 72h.

4.6.5 GelMA HYDROGEL SCAFFOLDS

The results obtained from the study of cell vitality and proliferation through direct cell culture on the plate led to the execution of a final experiment. This involved investigating the feasibility of culturing a scaffold inside the wells of the smart plate.

Working with a scaffold presents two potential aspects:

1. If it were possible to cultivate a scaffold within the wells, one could consider cultivating cells in this three-dimensional structure, thereby addressing the issue of poor cell proliferation observed in cells cultivated on the smart plate wells.
2. Considering one of the applications for which the device was developed, drug testing, the ability to create a three-dimensional cellular environment would enable more physiologically relevant testing.

In the context of drug testing, having a two-dimensional culture, where cells form a single layer, means that all cells are exposed to the same amount of drug, which does not replicate physiological conditions. The presence of a three-dimensional environment creates a gradient of the drug; thus, not all cells receive the same amount of drug, which mimics what happens *in vivo*.

For the creation of the scaffold, bovine-derived gelatin was functionalized with methacrylate groups to obtain methacrylated gelatin (GelMA). GelMA is widely used as a support structure for three-dimensional cell cultures due to its known biocompatibility. Once GelMA was obtained, before heating it to 37°C and pouring it into the wells, a stainless steel needle with a diameter of 0.7 mm was used to occlude the channels (Figure 4.36) and prevent GelMA from diffusing into them. After placing GelMA into the wells and allowing it to gel, the needle was removed, and a flow of ddH₂O solution with Disperse Blue 1 was started to observe the process. After the flow was completed, the scaffold was removed, and as shown in Figure 4.38, the scaffold allowed the solution to flow through. This is evidenced by the presence of the blue line inside the GelMA scaffold. Additionally, in the same figure, the maintenance of the channels can be observed.



Figure 4.36 Occlusion channels of the smart plate cona go of stainless steel with diameter $d=0.7$ mm

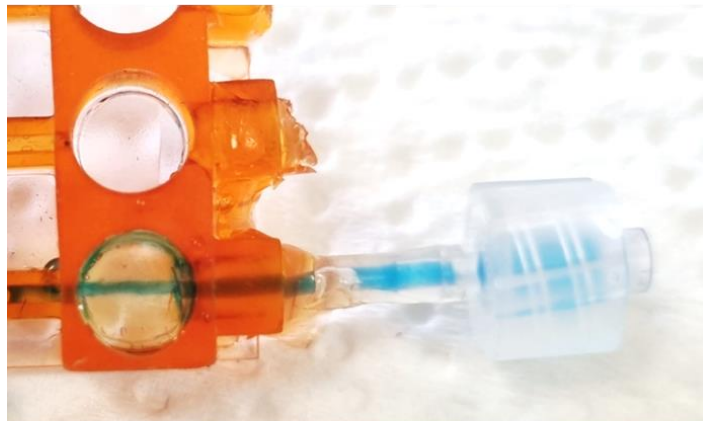


Figure 4.37 Flow within the scaffold grown in the smart plate

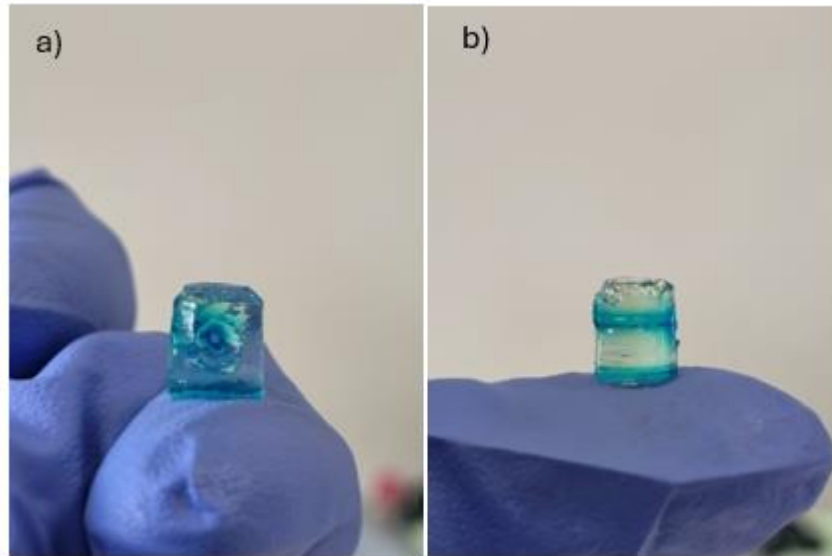


Figure 4.38 a) Maintaining channel openness and b) flow line within the scaffold

Although, due to timing constraints, it was not possible to conduct biological studies on these three-dimensional structures, achieving the scaffold, maintaining the openness of the channels, and facilitating flow passage highlighted the potential of the device for conduction studies on three-dimensional cultures.

CHAPTER 5: CONCLUSIONS

This thesis aimed to develop a 3D-printed device for cell culture and drug testing. We can divide the work into three distinct phases:

1. ***Printability of the Device Using Digital Light Processing (DLP) by employing various formulations:*** This phase required a study of different dyes to achieve free-flowing fluidic structures, enabling the flow of solutions such as culture media, drugs, or other soluble substances.
2. ***Study of Device Fluidics:*** The second phase involved studying the fluidics of the device. Solidworks and Comsol software were utilized to simulate and analyze the stresses experienced by cells under flow conditions. Additionally, direct flow passage tests were conducted on the device obtained from simulations.
3. ***Bio-Applications of the Device:*** The final phase focused on potential bio-applications of the device. This included material characterization and direct cellular studies conducted on the device to explore its suitability for biological applications.

In the first phase of the work, we succeeded in determining the formulations necessary to create a two-material device. This design aimed to provide sections of the device (device base and well base) that promote cell adhesion, while other sections (well walls and microfluidic structures) inhibit cell adhesion without inducing cytotoxic effects. Specifically, we chose to use a PEGDA-based formulation to enhance cell adhesion, and a TEGORad-based formulation to inhibit it. Subsequently, optimization of printing parameters enabled the creation of a 3D-printed device. Additionally, during this initial phase, we developed a functional washing protocol for the device to ensure its suitability for BIO applications.

In the second phase, our focus shifted to studying the fluidics of the device. The results obtained from simulations and direct tests on the smart plate assure us of the viability of using this plate for dynamic cell cultures.

In the final phase, our focus was on testing the actual feasibility of working within the BIO context without inducing cytotoxic effects. Cytotoxicity was indeed one of the first aspects studied through conditioned media tests. This type of test confirmed the non-cytotoxic nature of the material, allowing us to work with the smart plate directly in contact with cells. However, despite these initial results, when cells were cultured on the smart plate, they underwent cell death after more than 24 hours. To overcome this issue, we then explored the possibility of cultivating scaffolds within the smart plate using GelMA, one of the most commonly used materials in literature for creating scaffolds for cell cultures. Additionally, during this phase, we investigated the feasibility of using the same analytical instrumentation as used with the polystyrene plate. Specifically, we studied the potential autofluorescence of the

smart plate using the plate reader. We compared the signals emitted by the polystyrene and smart plates, obtaining comparable values between them. This allowed us to conclude that the smart plate can indeed be used with the plate reader to conduct certain experiments.

In order to improve the device developed in this thesis work, one could consider:

1. Performing further characterizations of the smart plate to obtain more information regarding the reasons why cells cultured on the smart plate wells underwent cell death.
2. Exploring possible functionalizations of the plate to enhance its bioactivity.
3. Conducting additional cellular assays and performing 3D cell culture experiments.
4. Investigating the interaction between drugs and the chosen device material to enable drug testing on both 2D and 3D cell cultures.

REFERENCES

- [1] M. Kapałczyńska *et al.*, “2D and 3D cell cultures – a comparison of different types of cancer cell cultures,” *Archives of Medical Science*, vol. 14, no. 4, pp. 910–919, 2018, doi: 10.5114/aoms.2016.63743.
- [2] K. Duval *et al.*, “Modeling physiological events in 2D vs. 3D cell culture,” *Physiology*, vol. 32, no. 4. American Physiological Society, pp. 266–277, Jun. 14, 2017. doi: 10.1152/physiol.00036.2016.
- [3] N. Fekete, A. V. Béland, K. Campbell, S. L. Clark, and C. A. Hoesli, “Bags versus flasks: a comparison of cell culture systems for the production of dendritic cell–based immunotherapies,” *Transfusion*, vol. 58, no. 7. Blackwell Publishing Inc., pp. 1800–1813, Jul. 01, 2018. doi: 10.1111/trf.14621.
- [4] C. Jensen and Y. Teng, “Is It Time to Start Transitioning From 2D to 3D Cell Culture?,” *Frontiers in Molecular Biosciences*, vol. 7. Frontiers Media S.A., Mar. 06, 2020. doi: 10.3389/fmolb.2020.00033.
- [5] G. Bassi, M. A. Grimaudo, S. Panseri, and M. Montesi, “Advanced multi-dimensional cellular models as emerging reality to reproduce In Vitro the human body complexity,” *International Journal of Molecular Sciences*, vol. 22, no. 3. MDPI AG, pp. 1–28, Feb. 01, 2021. doi: 10.3390/ijms22031195.
- [6] A. Cacciamali, R. Villa, and S. Dotti, “3D Cell Cultures: Evolution of an Ancient Tool for New Applications,” *Frontiers in Physiology*, vol. 13. Frontiers Media S.A., Jul. 22, 2022. doi: 10.3389/fphys.2022.836480.
- [7] M. Sun *et al.*, “3D Cell Culture—Can It Be As Popular as 2D Cell Culture?,” *Advanced NanoBiomed Research*, vol. 1, no. 5. John Wiley and Sons Inc, May 01, 2021. doi: 10.1002/anbr.202000066.
- [8] D. Huh, G. A. Hamilton, and D. E. Ingber, “From 3D cell culture to organs-on-chips,” *Trends in Cell Biology*, vol. 21, no. 12. pp. 745–754, Dec. 2011. doi: 10.1016/j.tcb.2011.09.005.
- [9] R. Edmondson, J. J. Broglie, A. F. Adcock, and L. Yang, “Three-dimensional cell culture systems and their applications in drug discovery and cell-based biosensors,” *Assay and Drug Development Technologies*, vol. 12, no. 4. Mary Ann Liebert Inc., pp. 207–218, May 01, 2014. doi: 10.1089/adt.2014.573.
- [10] B. Kumar, A. Prakash, R. K. Ruhela, and B. Medhi, “Potential of metabolomics in preclinical and clinical drug development,” *Pharmacological Reports*, vol. 66, no. 6. Elsevier B.V., pp. 956–963, 2014. doi: 10.1016/j.pharep.2014.06.010.
- [11] L. E. Knudsen, A. Smith, E. Törnqvist, A. Forsby, and H. Tähti, “Nordic symposium on ‘toxicology and pharmacology without animal experiments—Will it be possible in the next 10 years?’,” *Basic and Clinical Pharmacology*

- and Toxicology*, vol. 124, no. 5. Blackwell Publishing Ltd, pp. 560–567, May 01, 2019. doi: 10.1111/bcpt.13193.
- [12] M. Vinci *et al.*, “Advances in establishment and analysis of three-dimensional tumor spheroid-based functional assays for target validation and drug evaluation,” *BMC Biol*, vol. 10, Mar. 2012, doi: 10.1186/1741-7007-10-29.
- [13] D. Loessner, K. S. Stok, M. P. Lutolf, D. W. Hutmacher, J. A. Clements, and S. C. Rizzi, “Bioengineered 3D platform to explore cell-ECM interactions and drug resistance of epithelial ovarian cancer cells,” *Biomaterials*, vol. 31, no. 32, pp. 8494–8506, Nov. 2010, doi: 10.1016/j.biomaterials.2010.07.064.
- [14] V. Foglizzo, E. Cocco, and S. Marchiò, “Advanced Cellular Models for Preclinical Drug Testing: From 2D Cultures to Organ-on-a-Chip Technology,” *Cancers*, vol. 14, no. 15. MDPI, Aug. 01, 2022. doi: 10.3390/cancers14153692.
- [15] “Introduction: The Origin, Current Status, and Future of Microfluidics,” 2018.
- [16] L. Devries *et al.*, “Microfluidics-a review You may also like Distributed flow estimation and closed-loop control of an underwater vehicle with a multi-modal artificial lateral line 1 Microfluidics-a review.”
- [17] M. Tehranirokh, A. Z. Kouzani, P. S. Francis, and J. R. Kanwar, “Microfluidic devices for cell cultivation and proliferation,” *Biomicrofluidics*, vol. 7, no. 5, Sep. 2013, doi: 10.1063/1.4826935.
- [18] C. Regnault, D. S. Dheeman, and A. Hochstetter, “Microfluidic devices for drug assays,” *High-Throughput*, vol. 7, no. 2. MDPI AG, Jun. 01, 2018. doi: 10.3390/HT7020018.
- [19] J. Voldman, M. L. Gray, and M. A. Schmidt, “Microfabrication in Biology and Medicine,” 1999.
- [20] Y. Xia and G. M. Whitesides, “SOFT LITHOGRAPHY,” 1998. [Online]. Available: www.annualreviews.org
- [21] C. M. B. Ho, S. H. Ng, K. H. H. Li, and Y. J. Yoon, “3D printed microfluidics for biological applications,” *Lab on a Chip*, vol. 15, no. 18. Royal Society of Chemistry, pp. 3627–3637, Jul. 22, 2015. doi: 10.1039/c5lc00685f.
- [22] J. Friend and L. Yeo, “Fabrication of microfluidic devices using polydimethylsiloxane,” *Biomicrofluidics*, vol. 4, no. 2, 2010, doi: 10.1063/1.3259624.
- [23] R. Dong, Y. Liu, L. Mou, J. Deng, and X. Jiang, “Microfluidics-Based Biomaterials and Biodevices,” *Advanced Materials*, vol. 31, no. 45, Nov. 2019, doi: 10.1002/adma.201805033.
- [24] K. Raj M and S. Chakraborty, “PDMS microfluidics: A mini review,” *Journal of Applied Polymer Science*, vol. 137, no. 27. John Wiley and Sons Inc., Jul. 15, 2020. doi: 10.1002/app.48958.

- [25] T. D. Ngo, A. Kashani, G. Imbalzano, K. T. Q. Nguyen, and D. Hui, "Additive manufacturing (3D printing): A review of materials, methods, applications and challenges," *Composites Part B: Engineering*, vol. 143. Elsevier Ltd, pp. 172–196, Jun. 15, 2018. doi: 10.1016/j.compositesb.2018.02.012.
- [26] K. V. Wong and A. Hernandez, "A Review of Additive Manufacturing," *ISRN Mechanical Engineering*, vol. 2012, pp. 1–10, Aug. 2012, doi: 10.5402/2012/208760.
- [27] B. Bhushan and M. Caspers, "An overview of additive manufacturing (3D printing) for microfabrication," *Microsystem Technologies*, vol. 23, no. 4, pp. 1117–1124, Apr. 2017, doi: 10.1007/s00542-017-3342-8.
- [28] M. M. Prabhakar, A. K. Saravanan, A. H. Lenin, I. J. Leno, K. Mayandi, and P. S. Ramalingam, "A short review on 3D printing methods, process parameters and materials," in *Materials Today: Proceedings*, Elsevier Ltd, 2020, pp. 6108–6114. doi: 10.1016/j.matpr.2020.10.225.
- [29] R. Ranjan, D. Kumar, M. Kundu, and S. Chandra Moi, "A critical review on Classification of materials used in 3D printing process," *Mater Today Proc*, vol. 61, pp. 43–49, Jan. 2022, doi: 10.1016/j.matpr.2022.03.308.
- [30] I. Blanco, "The use of composite materials in 3d printing," *Journal of Composites Science*, vol. 4, no. 2. MDPI AG, 2020. doi: 10.3390/jcs4020042.
- [31] T. D. Ngo, A. Kashani, G. Imbalzano, K. T. Q. Nguyen, and D. Hui, "Additive manufacturing (3D printing): A review of materials, methods, applications and challenges," *Composites Part B: Engineering*, vol. 143. Elsevier Ltd, pp. 172–196, Jun. 15, 2018. doi: 10.1016/j.compositesb.2018.02.012.
- [32] O. Ivanova, C. Williams, and T. Campbell, "Additive manufacturing (AM) and nanotechnology: Promises and challenges," *Rapid Prototyp J*, vol. 19, no. 5, pp. 353–364, 2013, doi: 10.1108/RPJ-12-2011-0127.
- [33] I. Chiulan, E. B. Heggset, Ş. I. Voicu, and G. Chinga-Carrasco, "Photopolymerization of bio-based polymers in a biomedical engineering perspective," *Biomacromolecules*, vol. 22, no. 5. American Chemical Society, pp. 1795–1814, May 10, 2021. doi: 10.1021/acs.biomac.0c01745.
- [34] D. M. Zuev, A. K. Nguyen, V. I. Putlyaev, and R. J. Narayan, "3D printing and bioprinting using multiphoton lithography," *Bioprinting*, vol. 20. Elsevier B.V., Dec. 01, 2020. doi: 10.1016/j.bprint.2020.e00090.
- [35] L. Hontis, M. Van Der Borght, D. Vanderzande, and J. Gelan, "Radical as well as anionic polymerisation mechanisms in the synthesis of poly(p-arylene vinylene) precursors."
- [36] S. M. Müller, S. Schlögl, T. Wiesner, M. Haas, and T. Griesser, "Recent Advances in Type I Photoinitiators for Visible Light Induced Photopolymerization," *ChemPhotoChem*, vol. 6, no. 11. John Wiley and Sons Inc, Nov. 01, 2022. doi: 10.1002/cptc.202200091.

- [37] I. A. Timofticiuc *et al.*, “Biomaterials Adapted to Vat Photopolymerization in 3D Printing: Characteristics and Medical Applications,” *Journal of Functional Biomaterials*, vol. 15, no. 1. Multidisciplinary Digital Publishing Institute (MDPI), Jan. 01, 2024. doi: 10.3390/jfb15010007.
- [38] Y. Zhu *et al.*, “3D printing biomimetic materials and structures for biomedical applications,” *Bio-Design and Manufacturing*, vol. 4, no. 2. Springer, pp. 405–428, Jun. 01, 2021. doi: 10.1007/s42242-020-00117-0.
- [39] G. González *et al.*, “Materials testing for the development of biocompatible devices through vat-polymerization 3d printing,” *Nanomaterials*, vol. 10, no. 9, pp. 1–13, Sep. 2020, doi: 10.3390/nano10091788.
- [40] I. G. Siller *et al.*, “Characterization of a customized 3D-printed cell culture system using clear, translucent acrylate that enables optical online monitoring,” *Biomedical Materials (Bristol)*, vol. 15, no. 5, Sep. 2020, doi: 10.1088/1748-605X/ab8e97.
- [41] Z. Nejedlá *et al.*, “Class II biocompatible E-Shell 300 3D printing material causes severe developmental toxicity in: Danio rerio embryos and reduced cell proliferation in vitro -implications for 3D printed microfluidics,” *RSC Adv*, vol. 11, no. 27, pp. 16252–16267, Apr. 2021, doi: 10.1039/d1ra00305d.
- [42] N. Rekowska *et al.*, “Thermal, Mechanical and Biocompatibility Analyses of Photochemically Polymerized PEGDA250 for Photopolymerization-Based Manufacturing Processes,” *Pharmaceutics*, vol. 14, no. 3, Mar. 2022, doi: 10.3390/pharmaceutics14030628.
- [43] SigmaAldrich,
“[https://support.asiga.com/pico-2-hd/](https://www.bing.com/search?pglt=41&q=sigma+aldrich&cvid=ddb4824f13cd4b91a2c9dff61677158&gs_lcrp=EgZjaHJvbWUqBggAEEUYOzIGCAAQR Rg7MgYIARBFQDkyBggCEAAYQDIGCAMQABhAMgYIBBAAGEAyBggFEAAYQDIGCAYQABhAMgYIBxAAGEAyBggIEEUYPNIBBzk4NGowajGoAgCw AgA&FORM=ANNTA1&DAFO=1&PC=LCTS.””</p>
<p>[44] S. Villata <i>et al.</i>, “3D printable acrylate polydimethylsiloxane resins for cell culture and drug testing,” <i>Biomater Sci</i>, vol. 11, no. 8, pp. 2950–2959, Mar. 2023, doi: 10.1039/d3bm00152k.</p>
<p>[45] Asiga customer, “Asiga Pico 2 / HD.” Accessed: Jun. 27, 2024. [Online]. Available: <a href=)
- [46] IVTech, “LiveFlow 2-head Peristaltic Pump .”
- [47] I. Oshina and J. Spigulis, “Beer–Lambert law for optical tissue diagnostics: current state of the art and the main limitations,” *J Biomed Opt*, vol. 26, no. 10, Oct. 2021, doi: 10.1117/1.jbo.26.10.100901.
- [48] Agilent, “BioTek Synergy HTX Multimode Reader.”
- [49] Nikon Instruments Inc., “Nikon CSU-X1 Spinning Disk System .”

- [50] K. D. Kelley, L. Q. Olive, A. Hadziselimovic, and C. R. Sanders, "Look and see if it is time to induce protein expression in escherichia coli cultures," *Biochemistry*, vol. 49, no. 26, pp. 5405–5407, Jul. 2010, doi: 10.1021/bi1007194.
- [51] S. Yamashoji, A. Al Mamun, and L. Bari, "Visual and simple determination of glucose-induced acidification by yeast cells: application to rapid cytotoxicity test," *Heliyon*, vol. 6, no. 5, May 2020, doi: 10.1016/j.heliyon.2020.e03924.